	Shirai T, Ohara O, Fujita T, Heike T.			
Basophil-derived interleukin-4 controls the function of natural helper cells, a member of ILC2s, in lung inflammation	Motomura Y, Morita H, Moro K, Nakae S, Artis D, Endo TA, Kuroki Y, Ohara O, Koyasu S, Kubo M	Immunity. 40(5):758-71	2014	国外
遺伝子構造解析の現状とデータ解析アプローチ	小原　收	小児内科　46: 1545-1549	2014	国内
Highly efficient targeted mutagenesisin one-cell mouse embryos mediated by the TALEN and CRISPR/Cas systems	Yasue A, Mitsui SN, Watanabe T, Sakuma T, Oyadomari S, Yamamoto T, Noji S, Mito T, Tanaka E.	Sci Rep 4:5705	2014	国外

Ⅳ　研究成果の刊行物・別刷

Temporal Lineage Tracing of Aire-Expressing Cells Reveals a Requirement for Aire in Their Maturation Program

Yumiko Nishikawa,* Hitoshi Nishijima,* Minoru Matsumoto,* Junko Morimoto,* Fumiko Hirota,* Satoru Takahashi,† Hervé Luche,‡ Hans Joerg Fehling,‡ Yasuhiro Mouri,* and Mitsuru Matsumoto*,§

Understanding the cellular dynamics of Aire-expressing lineage(s) among medullary thymic epithelial cells (AEL-mTECs) is essential for gaining insight into the roles of Aire in establishment of self-tolerance. In this study, we monitored the maturation program of AEL-mTECs by temporal lineage tracing, in which bacterial artificial chromosome transgenic mice expressing tamoxifen-inducible Cre recombinase under control of the Aire regulatory element were crossed with reporter strains. We estimated that the half-life of AEL-mTECs subsequent to Aire expression was ~7–8 d, which was much longer than that reported previously, owing to the existence of a post-Aire stage. We found that loss of Aire did not alter the overall lifespan of AEL-mTECs, inconsistent with the previous notion that Aire expression in medullary thymic epithelial cells (mTECs) might result in their apoptosis for efficient cross-presentation of self-antigens expressed by AEL-mTECs. In contrast, Aire was required for the full maturation program of AEL-mTECs, as exemplified by the lack of physiological downregulation of CD80 during the post-Aire stage in Aire-deficient mice, thus accounting for the abnormally increased CD80^{high} mTECs seen in such mice. Of interest, increased CD80^{high} mTECs in Aire-deficient mice were not mTEC autonomous and were dependent on cross-talk with thymocytes. These results further support the roles of Aire in the differentiation program of AEL-mTECs. *The Journal of Immunology*, **2014, 192: 2585–2592.**

Studies of autoimmune disease are hampered by the complex influence of many factors, such as genetics, environmental microbial pathogens, age, and sex, which, either alone or in combination, can contribute to the development and pathogenesis of autoimmunity. For this reason, the mechanisms underlying the autoimmune disease caused by Aire deficiency, a monogenic organ-specific autoimmune disorder, have been a focus of intense research as a relatively simple model of autoimmune pathogenesis (1). Studies of *Aire* gene function could also help to answer the fundamental question of how the immune system discriminates between self and non-self within the thymic microenvironment. In this context, the discovery of Aire-dependent transcriptional control of a large number of tissue-restricted Ag (TRA) genes from medullary thymic epithelial cells (mTECs), where Aire is expressed most strongly (2), has created an attractive model suggesting that the primary role of Aire in establishment of self-tolerance is activation of TRA gene expression required for the negative selection of autoreactive T cells. Consequently, this model has encouraged many studies of Aire in an attempt to clarify how the single *Aire* gene can influence the transcription of such a large number of TRAs within mTECs (3–5).

In comparison with the remarkable changes noted in the expression profiles of TRA genes in Aire-deficient mTECs, morphological alterations in the medullary components from Aire-deficient mice were not initially appreciated. However, fairly recent detailed studies of Aire-deficient thymi have revealed several important aspects of the Aire-dependent differentiation programs of mTECs (6), such as increased numbers of mTECs with a globular cell shape (7, 8) and, in contrast, reduced numbers of terminally differentiated mTECs expressing involucrin, the latter being associated with reduced numbers of Hassall's corpuscles (8, 9). Although not fully investigated, increased percentages of mTECs expressing CD80 at high levels (CD80^{high}) is another suggested aspect of the Aire-dependent mTEC differentiation program (10–12). All of these findings together illuminate the importance of a full understanding of the Aire-dependent maturation process of the Aire-expressing lineage of medullary thymic epithelial cells (AEL-mTECs). It is noteworthy that the Aire-dependent mTEC differentiation program can be linked with the control of TRA gene expression, in which Aire may play a role from a different viewpoint (6). For example, given that acquisition of the properties of TRA gene expression depends on the maturation status of mTECs (13, 14), any defect in such an Aire-dependent maturation program could also account for defects of TRA gene expression in Aire-deficient mTECs. Thus, a precise understanding of the roles of Aire in mTEC differentiation is essential for clarification of Aire-dependent TRA gene expression and, ultimately, the roles of Aire in establishment of self-tolerance.

Another enigmatic aspect of Aire function is whether Aire exerts any proapoptotic activity within cells. It is believed that mTECs contribute to self-antigen expression by being phagocytosed by professional APCs at the expense of their death (i.e., cross-

*Division of Molecular Immunology, Institute for Enzyme Research, University of Tokushima, Tokushima 770-8503, Japan; †Institute of Basic Medical Sciences and Laboratory Animal Resource Center, Center for Tsukuba Advanced Research Alliance, University of Tsukuba, Tsukuba 305-8575, Japan; ‡Institute of Immunology, University Clinics Ulm, 89081 Ulm, Germany; and §Japan Science and Technology Agency, Core Research for Evolutional Science and Technology, 102-8666 Tokyo, Japan

Received for publication October 15, 2013. Accepted for publication January 12, 2014.

This work was supported in part by Grants-in-Aid for Scientific Research from the Japan Society for the Promotion of Science and from the Ministry of Education, Culture, Sports, Science and Technology of Japan, and CREST, the Japan Science Technology Agency (to M.M.).

Address correspondence and reprint requests to Prof. Mitsuru Matsumoto, Division of Molecular Immunology, Institute for Enzyme Research, University of Tokushima, 3-18-15 Kuramoto, Tokushima 770-8503, Japan. E-mail address: mitsuru@ier.tokushima-u.ac.jp

Abbreviations used in this article: AEL-mTEC, Aire-expressing lineage of medullary thymic epithelial cell; BAC, bacterial artificial chromosome; EGFP, enhanced GFP; EpCAM, epithelial cell adhesion molecule 1; mTEC, medullary thymic epithelial cell; tdRFP, tandem-dimer red fluorescent protein; Tg, transgenic; TRA, tissue-restricted Ag; UEA-1, *Ulex europaeus* agglutinin 1.

www.jimmunol.org/cgi/doi/10.4049/jimmunol.1302786

presentation; Ref. 14). In line with this notion, we have observed that many AEL-mTECs are in close contact with thymic DCs, suggesting efficient cross-presentation of TRAs from AEL-mTECs (15). Nevertheless, the issue of whether Aire itself exerts any pro-apoptotic activities has not been directly addressed using an in vivo system. The proapoptotic activity of Aire has been deduced in part from the increased proportion of the $CD80^{high}$ mTEC population (in which $Aire^+$ mTECs reside) in Aire-deficient mice, despite the lack of ability by Aire to directly cause proliferative arrest of mTECs (10).

Finally, a conflicting idea has come to light that Aire can either inhibit or promote the differentiation program of AEL-mTECs (6). The inhibition model assumes that only an absence of Aire would reveal the full program of terminal differentiation of AEL-mTECs (16). It is important to note that this model was constructed based partly on the concept of the proposed proapoptotic activity of Aire. In contrast, we have suggested that Aire helps to promote the differentiation program in AEL-mTECs, and this model assumes defective accomplishment of the differentiation program in the absence of Aire, associated with impaired expression of the TRA gene in AEL-mTECs through the mechanisms described above (6, 8).

One important step toward clarifying these issues is to compare the maturation-associated cell signatures and lifespan of AEL-mTECs in either the presence or the absence of Aire, using in vivo models. Although lineage tracing (or fate mapping) is a particularly powerful strategy for this purpose, the conventional approach does not allow us to chase the developmental process of AEL-mTECs because Aire is expressed before emergence of the three germ cell layers, prior to its thymic expression (15). To overcome this problem, we have developed a timing-controlled lineage-tracing system that allows permanent marking of AEL-mTECs with fluorescent proteins. This approach for investigating the cellular dynamics of AEL-mTECs by temporal lineage tracing has revealed many fundamental and previously unknown characteristics of AEL-mTECs.

Materials and Methods

Mice

A bacterial artificial chromosome (BAC) transgenic (Tg) construct containing 97.1 kb of the 5′ region and 69 kb of the 3′ region flanking the *Aire* gene was generated from BAC clone RP23-461E7, in which the *Aire* start codon was replaced with an open reading frame encoding a tamoxifen-inducible Cre recombinase (17) followed by a poly-A signal from the rabbit *β globin* gene. Aire/CreER BAC Tg mice were generated by injecting a linearized BAC Tg construct into pronuclei of fertilized C57BL/6 oocytes, and Tg founders were chosen by Southern blot analysis. A reporter Tg strain expressing enhanced GFP (EGFP) upon Cre-mediated recombination (CAG-CAT-EGFP, line 39) (18), a knockin Cre reporter strain expressing a tandem-dimer red fluorescent protein (tdRFP) (19), and Aire/GFP knockin mice (8) were generated as described previously. For induction of Cre recombinase activity, mice were given 500 μg tamoxifen dissolved in 50 μl corn oil i.p. for 6 d. The day after that, on which mice received the final dose of tamoxifen, was counted as day 1. Rag2-deficient mice on a C57BL/6 background were purchased from Taconic. All mice were maintained under pathogen-free conditions. The protocols used in this study were in accordance with the Guidelines for Animal Experimentation of Tokushima University School of Medicine, Tokushima, Japan.

Immunohistochemistry

Immunohistochemical analysis of the thymus with goat polyclonal anti-GFP Ab (Nobus Biologicals), rabbit polyclonal anti-GFP Ab (Invitrogen), anti–epithelial cell adhesion molecule 1 (EpCAM) mAb (BD), anti-Ly51 mAb (eBioscience), and rat anti-Aire mAb (clone RF33-1) was performed as described previously (8, 15).

TEC preparation and flow cytometric analysis

Preparation of TECs and flow cytometric analysis with a FACScalibur (BD) and a FACSAria II (BD) were performed as described previously (8, 15). The mAbs used were anti-CD45 and anti-CD80, both purchased from eBioscience. *Ulex europaeus* agglutinin 1 (UEA-1) was from Vector Laboratories. Rat anti-Aire mAb was clone RF33-1 prepared in our laboratory.

Results

Characterization of the post-Aire mTEC differentiation program by temporal lineage tracing

Because of Aire expression in the early embryo, it is impossible to perform lineage tracing of AEL-mTECs with a conventional fate-mapping system (15). We sought to overcome this problem by generating BAC Tg mice expressing tamoxifen-inducible Cre recombinase under control of the Aire regulatory element (Aire/CreER BAC Tg), allowing induction of Cre recombinase activity at will (Fig. 1A). One Aire/CreER BAC Tg line was established, and this was crossed with a reporter Tg strain expressing EGFP (CAG-CAT-EGFP) (18) (Fig. 1A) or tdRFP (19) (not depicted in Fig. 1A) upon Cre-mediated recombination. We first performed immunohistochemistry with anti-GFP Ab to monitor GFP expression in the thymus from double-Tg mice 1 d after tamoxifen treatment. We observed many GFP^+ cells that were confined to the thymic medulla (i.e., $Ly51^-$ areas) (Fig. 1B), and approximately one- to two-thirds of the cells coexpressed endogenous Aire protein (Fig. 1C). No GFP^+ cells were observed in the absence of tamoxifen treatment (data not shown). We also used flow cytometric analysis for detection of GFP signals, together with expression of Aire protein in mTECs at different time points after tamoxifen treatment. Just after tamoxifen treatment, ~30% of the GFP^+ cells expressed endogenous Aire, and these cells were almost exclusively from the $CD80^{high}$ population (Fig. 1D). In contrast, none of the GFP^+ cells expressed Aire protein 11 d after tamoxifen treatment, indicating that these cells corresponded to post-Aire mTECs at this later time point. We did not observe any GFP^+ cells outside the thymus, including the spleen and lymph nodes, after tamoxifen treatment (Y. Nishikawa and M. Matsumoto, unpublished observations). These results confirmed that we were able to mark the AEL-mTECs reproducibly with this Aire/CreER BAC Tg line to monitor the process of AEL-mTEC maturation.

We then investigated the kinetics of the disappearance of AEL-mTECs from the thymus after tamoxifen treatment by assessing the proportion of GFP^+ cells among mTECs on an Aire-sufficient background (Fig. 2A). The proportion of GFP^+ cells gradually decreased with time after tamoxifen treatment, and by 3 wk they had almost disappeared from the thymus. Given that transcriptional blockade of the *Aire* gene in a doxycycline-inducible Aire turnoff Tg system results in the disappearance of $Aire^+$ mTECs over the following 3–5 d (20), it seems reasonable to speculate that the lifespan of Aire protein, once expressed, is < 1 wk. The fact that the total disappearance of AEL-mTECs (GFP^+ cells) from the thymus took 3 wk from the initial tamoxifen treatment in our temporal lineage-tracing system suggests that there is a significant post-Aire period ($\leq$2 wk) when AEL-mTECs have terminated *Aire* gene transcription until they finally disappear from the thymus. We estimated the half-life of AEL-mTECs after activation of Cre recombinase activity to be ~8 and 7 d using the CAG-CAT-EGFP (Fig. 2A) and tdRFP reporter strains (Fig. 2C), respectively. It is noteworthy that these estimated times were almost twice as long as those reported previously (i.e., 3–4 d) (10), which would not have accounted for the existence of a post-Aire stage for AEL-mTECs because anti-Aire Ab was used for monitoring.

Dispensable role of Aire in inducing apoptosis of AEL-mTECs

A model has been suggested in which Aire concomitantly induces apoptosis in mTECs, thereby promoting cross-presentation of

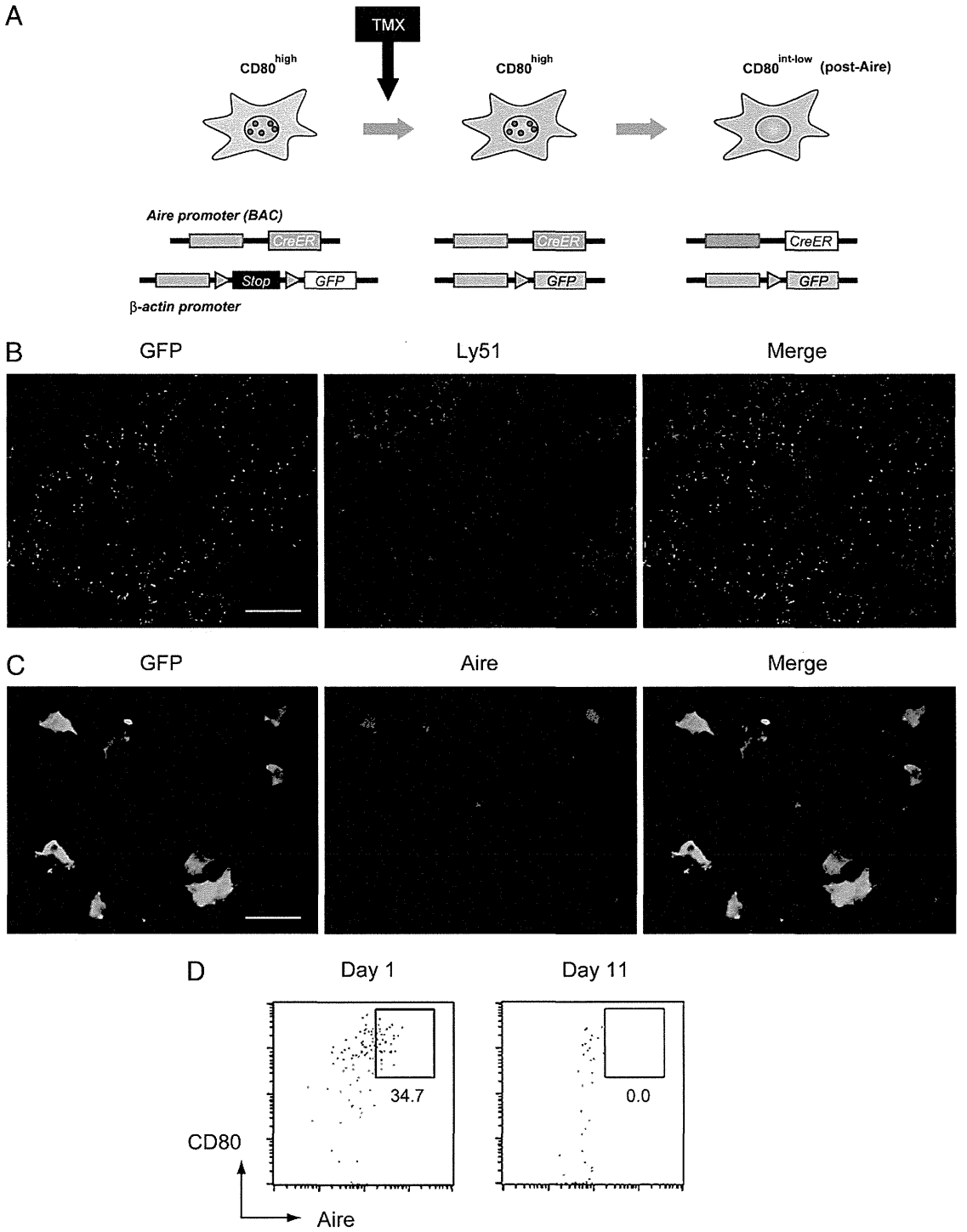

FIGURE 1. Experimental design for the temporal lineage tracing of Aire-expressing mTECs and its specificity. (**A**) A BAC Tg expressing tamoxifen-inducible Cre recombinase under the control of the Aire regulatory element (Aire/CreER BAC Tg) was generated. After crossing with reporter strains expressing GFP (CAG-CAT-EGFP) or RFP (tdRFP) (not depicted), tamoxifen was given i.p. to facilitate translocation of the Cre recombinase from the cytoplasm to the nucleus to activate the Cre-mediated recombination of the reporter genes. (**B**) GFP^+ cells (green) (*left*) were observed in the thymic medulla (negative for Ly51, stained red) (*center*) by immunohistochemistry upon treatment with tamoxifen. Thymi were removed 1 d after tamoxifen treatment. Scale bar, 500 μm. One representative experiment from a total of two repeats is shown. (**C**) Concomitant expression of GFP (green) and endogenous mouse Aire (red) was examined using anti-GFP Ab (*left*) and anti-Aire mAb (*center*), respectively. Scale bar, 20 μm. One representative experiment from a total of three repeats is shown. (**D**) Endogenous mouse Aire expression from GFP-marked cells was demonstrated by flow cytometric analysis. Thymic stromal cells were isolated enzymatically, and $CD45^-GFP^+$ cells were analyzed for expression of Aire together with CD80 at day 1 (*left*) and day 11 (*right*) after tamoxifen treatment. $Aire^+CD80^{high}$ cells were detected only at day 1 after tamoxifen treatment among the GFP^+ cells. Blue and red dots correspond to $CD80^{high}$ and $CD80^{intermediate\ to\ low}$ cells, respectively. Percentages of the cells in the indicated regions are included. One representative experiment from a total of three repeats is shown.

TRAs targeted by the transcriptional activity of Aire (10). However, our previous fate-mapping study revealed the existence of a post-Aire stage (15), and our present data show that in fact it is rather long, raising a question about the proapoptotic activity of Aire. To clarify this issue more directly, we compared the survival time of AEL-mTECs from Aire-sufficient and Aire-deficient mice,

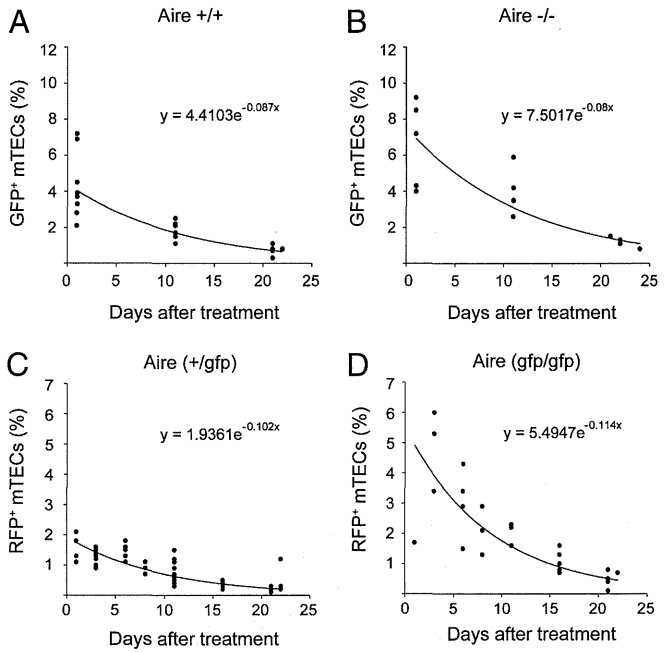

FIGURE 2. Lack of obvious proapoptotic activity of Aire within the Aire-expressing mTEC lineage. (**A**) Kinetic properties of the Aire-expressing mTEC lineage evaluated at different time points after tamoxifen treatment on an Aire-sufficient background. Percentages of GFP$^+$ Aire-expressing mTECs were evaluated from Aire/CreER BAC Tg crossed with CAG-CAT-EGFP, using flow cytometric analysis. Thymic stromal cells were gated for CD45$^-$EpCAM$^+$UEA-1$^+$ cells. Each circle corresponds to one mouse analyzed. The half-life of Aire-expressing mTECs in the presence of Aire was calculated as 8.0 d. An exponential trend line is given, $R^2 = 0.78$. Data were accumulated from a total of 10 experiments using 19 mice. (**B**) Kinetic properties of Aire-expressing mTECs in the absence of Aire. The half-life of Aire-expressing mTECs in the absence of Aire was calculated as 8.7 d. An exponential trend line is given, $R^2 = 0.83$. Data were accumulated from a total of 9 experiments using 13 mice. (**C** and **D**) Aire/CreER BAC Tg mice crossed with the tdRFP reporter mice were further crossed onto Aire/GFP knockin mice. Kinetic properties of Aire-expressing mTEC lineage evaluated at different time points after tamoxifen treatment on an Aire-sufficient ($Aire^{+/gfp}$) (C) and an Aire-deficient ($Aire^{gfp/gfp}$) background (D). The half-life of Aire-expressing mTECs on an Aire-sufficient and an Aire-deficient background was 6.8 and 6.1 d, respectively. Exponential trend lines are given, $R^2 = 0.70$ (for the Aire-sufficient background) and 0.71 (for the Aire-deficient background).

using the temporal lineage-tracing system described above, anticipating that if Aire has any proapoptotic activity, then the lifespan of AEL-mTECs would be prolonged by Aire deficiency within the cells. For this purpose, we further introduced an Aire-deficient background onto Aire/CreER BAC Tg crossed with CAG-CAT-EGFP. It was found that the half-life of AEL-mTECs showed no difference between an Aire-sufficient (i.e., 8.0 d estimated from Fig. 2A) and an Aire-deficient background (i.e., 8.7 d estimated from Fig. 2B), suggesting a lack of any obvious proapoptotic activity of Aire; throughout the observation period, we observed higher percentages of GFP$^+$ cells among the mTECs in an Aire-deficient background than was the case for those from an Aire-sufficient background. We speculate that this finding may reflect the augmented and/or prolonged transcriptional activity of the Aire locus in the absence of Aire itself, both resulting in higher efficiency of Cre-mediated recombination of the GFP reporter. No obvious alteration in the lifespan kinetics of AEL-mTECs resulting from lack of Aire was demonstrated by crossing Aire/CreER BAC Tg onto the tdRFP reporter strain, in which the effect was compared between heterozygous (i.e., 6.8 d, estimated from Fig. 2C) and homozygous Aire deficiency (i.e., 6.1 d, estimated from Fig. 2D). Thus, Aire itself seems to be irrelevant for efficient cross-presentation through its induction of apoptosis within AEL-mTECs.

Altered differentiation program of AEL-mTECs in the absence of Aire

Alteration of the differentiation program of AEL-mTECs in Aire-deficient mice has been suggested from the phenotypic changes exhibited by the mTECs, including increased numbers of cells with a globular shape (7, 8) and reduced numbers of terminally differentiated mTECs expressing involucrin, in association with reduced numbers of Hassall's corpuscles (8, 9). However, a more quantitatively noticeable change in the Aire-deficient thymic stroma was an increase of mTECs with a mature signature, expressing CD80 and MHC-II at high levels (10–12). Aire-deficient mice have an increased proportion and/or number of mTECs with high CD80 and MHC-II expression (i.e., mTEC^{high}), despite the fact that Aire does not have a direct impact on the division of mTECs, thus leading to the hypothesis that Aire has proapoptotic activity (10). However, the exact mechanism responsible for this phenotype remains unknown. We investigated the mechanisms underlying the possible link between increased CD80^{high} mTECs in Aire-deficient mice and alteration of the differentiation program of AEL-mTECs lacking Aire.

We first examined which type of cell, the Aire-expressing or non–Aire-expressing mTEC, is responsible for the increase of CD80^{high} mTECs. We used Aire/GFP knockin mice, because this strain allows us to discriminate between Aire-expressing and non–Aire-expressing lineages even on an Aire-deficient background (8). We assessed the expression of CD80 together with GFP after gating for CD45$^-$EpCAM$^+$UEA-1$^+$ mTECs. To exclude any gene-dosage effect of the GFP-expressing allele, we made a comparison between mice with the *+/gfp* ($Aire^{+/gfp}$) and *−/gfp* ($Aire^{-/gfp}$) genotypes. As reported previously (10–12) and exemplified in Fig. 3A, the total percentages of CD80^{high} mTECs were increased in Aire-deficient $Aire^{-/gfp}$ mice. Notably, this increase was not observed in the GFP$^+$CD80^{high} (Aire-expressing) population, but in the GFP$^-$CD80^{high} (non–Aire-expressing) population (Fig. 3A, Fig. 3B). This finding was rather unexpected because Aire$^+$ mTECs are a CD80^{high} population, and we had anticipated that, conversely, the increased percentages of CD80^{high} mTECs would have been made up of cell lineages expressing Aire.

Given that increased CD80^{high} mTECs in Aire-deficient mice were made up predominantly of non–Aire-expressing mTECs (including post-Aire mTECs), we suspected that these CD80^{high} mTECs from Aire-deficient mice might, for some reason, contain mTECs at the post-Aire stage, which normally exhibit downregulation of CD80 and MHC-II in the presence of Aire (15). Indeed, when the expression levels of CD80 were monitored after tamoxifen treatment in double-Tg mice (i.e., Aire/CreER BAC Tg crossed with CAG-CAT-EGFP), we found that they remained high during the observation period on an Aire-deficient background, whereas they gradually declined on an Aire-sufficient background (Fig. 3C). These results suggested that, in Aire-deficient mice, CD80 is abnormally sustained at a high level during the differentiation program of AEL-mTECs after Aire expression has been terminated (i.e., in the post-Aire stage). A similar pattern was observed when we examined the expression levels of MHC-II at the post-Aire stage (data not shown).

To further confirm that the increase in the number of CD80^{high} mTECs in Aire-deficient mice is due to lack of physiological downregulation of CD80 during the post-Aire stage, we applied the tamoxifen-inducible lineage-tracing system to $Aire^{+/gfp}$ mice,

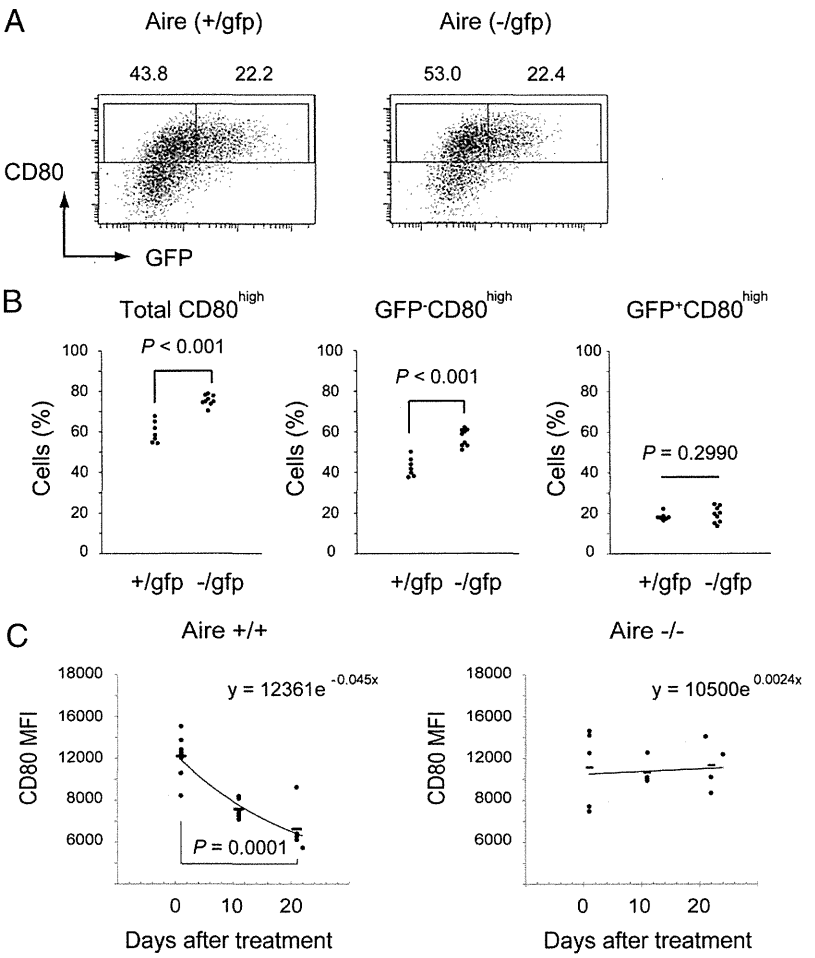

FIGURE 3. Altered differentiation program of AEL-mTECs in the absence of Aire. (**A**) Thymic stromal cells from Aire-sufficient (*Aire*$^{+/gfp}$) and Aire-deficient (*Aire*$^{-/gfp}$) mice were isolated enzymatically and evaluated for expression of CD80 and GFP after gating for CD45$^-$EpCAM$^+$UEA-1$^+$ cells. Percentages of the cells in the indicated regions are included. One representative experiment from a total of four repeats is shown. (**B**) Percentages of total CD80^{high} (*left*), GFP$^-$CD80^{high} (*center*), and GFP$^+$CD80^{high} (*right*) cells were plotted from a total of three experiments. Each circle corresponds to one mouse analyzed. (**C**) CD80 expression levels from temporal lineage tracing (i.e., GFP$^+$ cells) were monitored at different time points after tamoxifen treatment on both an Aire-sufficient (*left*) and an Aire-deficient (*right*) background. Mean fluorescence intensities (MFI) of CD80 were plotted. Each circle corresponds to one mouse analyzed. Gray lines represent mean values. An exponential trend line is given, $R^2 = 0.72$ for Aire-sufficient mice and $R^2 = 0.0009$ for Aire-deficient mice. Data were accumulated from a total of four experiments.

in which *Aire* gene transcription can be monitored by GFP expression on a real-time basis (8); we further introduced the *Aire*$^{+/gfp}$ allele into Aire/CreER BAC Tg crossed with the tdRFP reporter strain (Fig. 4A). In this system, GFP$^+$ cells (with active *Aire* gene transcription) should also express the tamoxifen-responsive *Cre* gene derived from the Aire/CreER BAC Tg allele, but the recombination activity of Cre for turning on the tdRFP signal becomes active only after tamoxifen treatment (see Fig. 2C and Fig. 2D for RFP expression from triple-Tg mice [i.e., Aire/CreER BAC Tg crossed with tdRFP reporter and Aire/GFP knockin mice]). Once exposed to tamoxifen, GFP$^+$ cells start to express the RFP signal and become GFP$^+$RFP$^+$ cells, and this condition persists until *Aire* gene transcription ceases (Fig. 4A). Eventually, the transcriptional activity of Aire will be lost (i.e., entry into the post-Aire stage), and the cells then become GFP$^-$RFP$^+$ cells. Thus, in this experimental setting, AEL-mTECs can be recognized according to the sequence of their maturation in the order (GFP$^+$RFP$^-$), GFP$^+$RFP$^+$, and GFP$^-$RFP$^+$.

We first validated this experimental system by assessing the fluorescence characteristics of AEL-mTECs at different time points after tamoxifen treatment. After tamoxifen treatment, we observed AEL-mTECs exhibiting all three fluorescence combinations in an Aire-sufficient (*Aire*$^{+/gfp}$) background (Fig. 4B). It was noteworthy that more GFP$^+$RFP$^+$ cells than GFP$^-$RFP$^+$ cells were observed among tamoxifen-responsive RFP$^+$ cells at an early stage of evaluation (1.3 versus 0.3% on day 3: Fig. 4B, *top left*), whereas we observed more GFP$^-$RFP$^+$ cells than GFP$^+$RFP$^+$ cells 11 d after tamoxifen treatment (0.4 versus 0.2% on day 11: Fig. 4B, *top right*), suggesting progressive maturation of AEL-mTECs with time. We then focused on the level of CD80 expression in GFP$^-$ RFP$^+$ cells, corresponding to mTECs at the post-Aire stage, from both an Aire-sufficient (*Aire*$^{+/gfp}$) and an Aire-deficient (*Air*$^{-/gfp}$) background. As a control, we evaluated the level of CD80 expression in GFP$^+$RFP$^-$ cells, representing an initial stage of Aire expression. We found that GFP$^+$RFP$^-$ cells from both *Aire*$^{+/gfp}$ and *Aire*$^{-/gfp}$ mice showed similar levels of CD80 expression throughout the analysis (i.e., at days 3 and 11 after tamoxifen treatment) (Fig. 4C). However, when we focused on the level of CD80 expression in GFP$^-$RFP$^+$ cells at 11 d after tamoxifen treatment, when most of the RFP-labeled AEL-mTECs would have been at the post-Aire stage, the level of CD80 expression in cells from *Aire*$^{-/gfp}$ mice was significantly higher than that of cells from *Aire*$^{+/gfp}$ mice (Fig. 4C, Fig. 4D). These CD80-sustaining post-Aire mTECs from Aire-deficient mice can be recognized as CD80^{high} mTECs, as observed in Fig. 3A. Thus, the increase of CD80^{high} mTECs in Aire-deficient mice was due to accumulation of cells, abnormally sustaining their expression of CD80^{high}, even at the post-Aire stage. These results further support our hypothesis that lack of Aire has an impact on the differentiation program of AEL-mTECs.

Cross-talk with mature thymocytes is required for the Aire-dependent differentiation program of AEL-mTECs

The program of mTEC maturation is influenced by many factors derived from developing thymocytes (e.g., TNF receptor family ligands, growth factors) (13). We examined whether cross-talk with thymocytes is required for the Aire-dependent differentiation program of AEL-mTECs described above. For this purpose, we investigated whether the increase of CD80^{high} mTECs in Aire-deficient mice would occur even in the absence of mature thy-

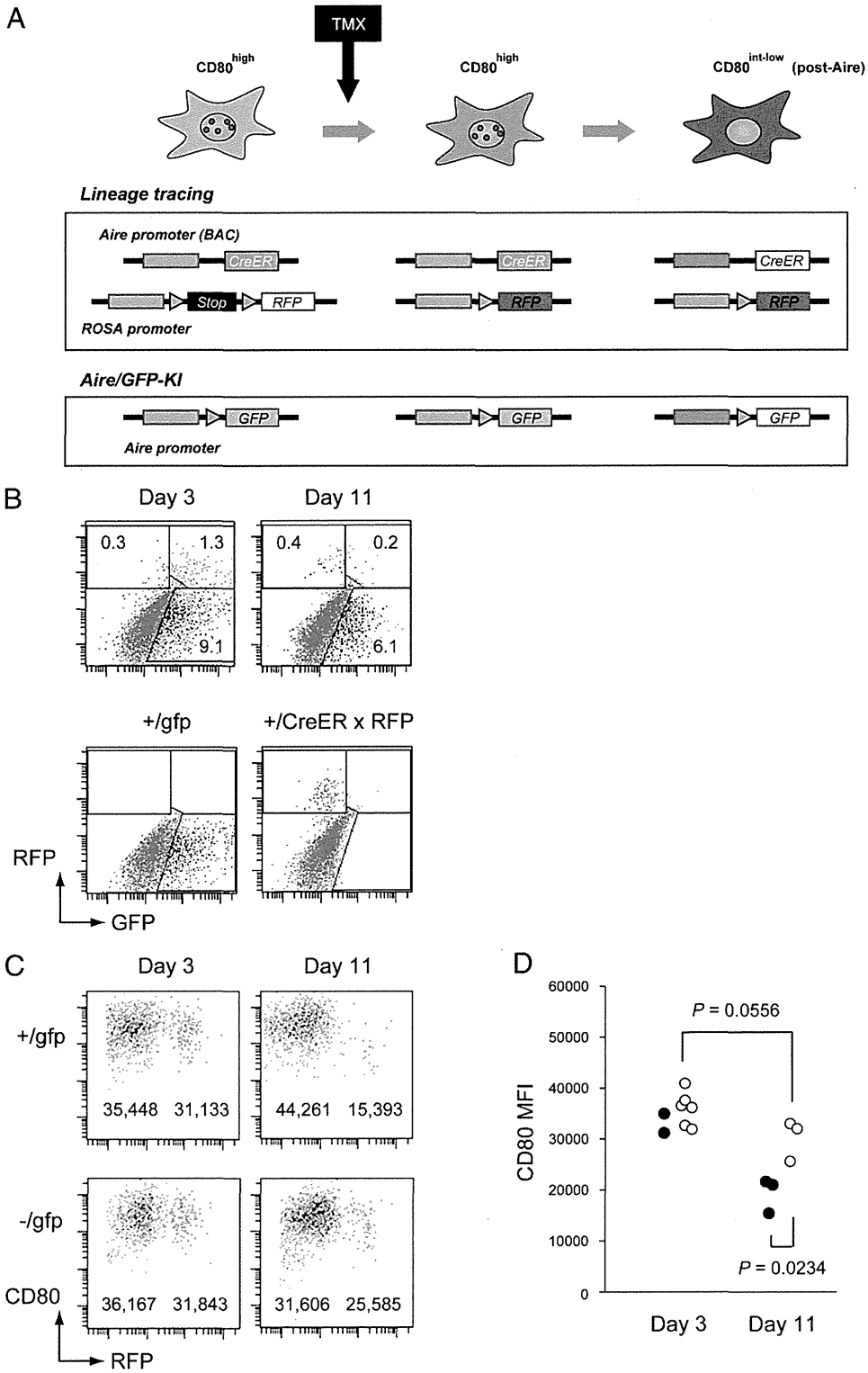

FIGURE 4. Defective physiological downregulation of CD80 on AEL-mTECs at the post-Aire stage in the absence of Aire. (**A**) Experimental design for the combination of temporal lineage tracing and Aire/GFP knockin mice for evaluation of the stage progression of Aire-expressing mTECs through their differentiation. Aire/CreER BAC Tg mice crossed with the tdRFP reporter were further crossed onto Aire/GFP knockin mice; these were finally crossed onto Aire-deficient mice to generate an Aire-deficient ($Aire^{-/gfp}$) background (not depicted). Upon treatment with tamoxifen, additional RFP expression onto the currently Aire-expressing GFP^+ mTECs made the cells GFP^+RFP^+ stage, followed by the GFP^-RFP^+ stage through loss of their ability to express Aire (GFP) at the post-Aire stage. (**B**) Thymic stromal cells from Aire-sufficient ($Aire^{+/gfp}$) mice crossed onto temporal lineage-tracing mice were evaluated for expression of GFP and RFP at different time points after tamoxifen treatment to show the stage progression of Aire-expressing mTECs during their differentiation (*top*). Representative profiles for the expression of GFP and RFP at days 3 and 11 after tamoxifen treatment are shown. Percentages of the cells in the indicated regions are included. Controls at day 3 showing the profiles from Aire/GFP knockin (in which only the GFP signal should be detected) (*bottom left*) and Aire/CreER BAC Tg mice crossed with the tdRFP reporter (in which only the RFP signal should be detected) (*bottom right*) for setting the gating windows were also shown. (**C**) Thymic stromal cells from Aire-sufficient ($Aire^{+/gfp}$) (*top*) and Aire-deficient ($Aire^{-/gfp}$) mice (*bottom*) were evaluated for expression of CD80 and RFP after gating for $CD45^-EpCAM^+UEA\text{-}1^+GFP^+$ or $CD45^-EpCAM^+UEA\text{-}1^+RFP^+$ cells; green *(Figure legend continues)*

mocytes by generating mice deficient in both Aire and Rag2. The proportions of CD80^{high} mTECs were much lower on a Rag2-deficient background (Fig. 5), being consistent with the much lower numbers of AEL-mTECs in Rag2-deficient mice (8). We found that the proportions of CD80^{high} mTECs were indistinguishable between Aire-sufficient and Aire-deficient mice on a Rag2-deficient background, suggesting that the differentiation program of AEL-mTECs may not be absolutely mTEC autonomous with regard to Aire dependency. Instead, cross-talk with mature thymocytes might also play an important role in the Aire-dependent differentiation program of AEL-mTECs.

Discussion

Our temporal lineage-tracing approach has enabled us to assess precisely the kinetic properties of AEL-mTECs, including their half-life subsequent to Aire expression (i.e., 7–8 d) and the length of the post-Aire stage (≤2 wk). Our approach has also helped to clarify a number of fundamental and previously unsolved issues related to AEL-mTECs, as follows. We found that Aire plays a neutral role in the induction of cell death among AEL-mTECs, although the roles of Aire in other aspects of cross-presentation per se (e.g., transfer of TRAs from AEL-mTECs to bone marrow–APC and/or the ability of bone marrow–APCs to present TRAs) need to be explored further. We also clarified the mechanisms responsible for the increase of CD80^{high} mTECs in Aire-deficient mice, which were found to reflect another defect in the differentiation program of AEL-mTECs resulting from lack of Aire.

We have demonstrated that the increase in the number of CD80^{high} mTECs in Aire-deficient mice was due, at least in part, to lack of physiological downregulation of CD80 during the post-Aire stage. This finding was first obtained by monitoring the levels of CD80 expression in gross lineage-traced cells at different time points after tamoxifen treatment (Fig. 3C). We then introduced the *Aire*$^{+/gfp}$ allele into Aire/CreER BAC Tg crossed with the tdRFP reporter strain to focus on the genuine post-Aire mTECs (i.e., GFP$^-$RFP$^+$ cells in Fig. 4), because GFP$^+$ cells in the initial analysis might also have included AEL-mTECs still possessing the Aire protein (as exemplified at day 1 in Fig. 1D). Although alterations in the ratios of GFP$^+$RFP$^+$ to GFP$^-$RFP$^+$ cells at different time points justified this experimental system, the lack of any discernible increase of GFP$^-$RFP$^+$ cells (from 0.3 to 0.4%) from day 3 to day 11, compared with the significant decrease of GFP$^+$RFP$^+$ cells (from 1.3 to 0.2%), also suggested a loss of GFP$^-$RFP$^+$ cells during the assay: post-Aire mTECs might be susceptible to death attributable to their physiological lifetime, and we suspect that some of the GFP$^-$RFP$^+$ cells might have already died and thus escaped from the analysis, especially at later time points. Obviously, post-Aire mTECs are a heterogeneous population, but the currently available fate-mapping approach does not allow us to discriminate each type of post-Aire mTEC for evaluation depending on the period traced. Accordingly, we analyzed the lineage-traced cells as a homogenous population by changing the time points of observation. We consider that development of novel experimental systems might be required to overcome some of the technical limitations of the current fate-mapping approach, thereby clarifying the dynamic nature of AEL-mTECs individually.

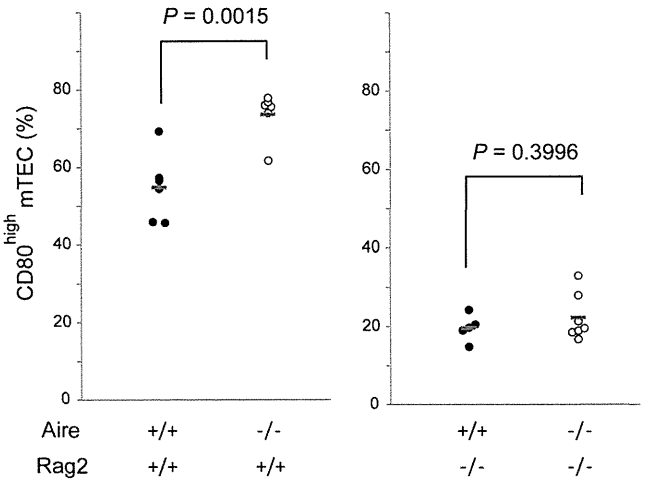

FIGURE 5. Cross-talk with mature thymocytes is required for the Aire-dependent differentiation program of AEL-mTECs. Thymic stromal cells from Aire-sufficient (solid circles) and Aire-deficient mice (clear circles) on either a Rag2-sufficient (*left*) or a Rag2-deficient background (*right*), aged 7 wk, were examined by flow cytometric analysis. Percentages of CD80^{high} cells after gating for CD45$^-$EpCAM$^+$UEA-1$^+$ mTECs are plotted. Each circle corresponds to one mouse analyzed. Gray lines represent mean values. Data were accumulated from a total of four experiments.

The defective physiological downregulation of CD80 at the post-Aire stage in the absence of Aire, as demonstrated in the current study, together with the reduced numbers of mTECs with mature signatures (8, 9), strongly suggests that Aire is a differentiation-promoting factor rather than one that inhibits the differentiation of AEL-mTECs (6). Given that the lifespan of AEL-mTECs remained unchanged in the absence of Aire, the present results suggest that Aire-deficient AEL-mTECs are lost from the thymus if the maturation signature is incomplete. However, the exact point in the differentiation process at which Aire-deficient mTECs are prevented from differentiating further still remains unclear. Investigation of this issue has been hampered by the current lack of suitable markers for the mTEC differentiation program: so far, CD80 and MHC-II remain the few that are available, and Aire expression may now be added to this profile. Precise elucidation of the target gene(s) relevant to the progression of mTEC differentiation controlled by Aire is an essential task to achieve a full understanding of the roles of Aire in the differentiation program of AEL-mTECs. From a broader viewpoint, future work will need to focus on how the Aire-dependent differentiation program of mTECs contributes to the generation of a tolerogenic thymic microenvironment.

Recently, Metzger et al. (21) developed a similar tamoxifen-inducible fate-mapping system, and confirmed the existence of a post-Aire stage. They found that the half-life of AEL-mTECs was longer than previously thought, as we have demonstrated in the current study. Of interest, their study also showed that Aire$^+$ mTECs had highly regenerative potential, and that the process depended on RANK signaling, as has been suggested for the production and/or maintenance of Aire$^+$ mTECs (9, 22). Furthermore, they reported that the spectrum of TRA genes expressed

and red dots are from the GFP$^+$RFP$^-$ and GFP$^-$RFP$^+$ populations, respectively. Representative profiles for the expression of CD80 and RFP at days 3 and 11 after tamoxifen treatment are shown. In Aire-deficient (*Aire*$^{-/gfp}$) mice, a significant proportion of RFP$^+$ cells remained CD80^{high} even at day 11. MFIs of CD80 in the indicated populations are included. One representative experiment from a total of three repeats is shown. (**D**) MFIs of CD80 from GFP$^-$RFP$^+$ populations at days 3 and 11 after tamoxifen treatment on an Aire-sufficient (*Aire*$^{+/gfp}$) (solid circles) and an Aire-deficient (*Aire*$^{-/gfp}$) (clear circles) background. Each circle corresponds to one mouse analyzed. Data were accumulated from a total of 3 experiments using 14 mice.

by post-Aire mTECs was different from that of mTECs with ongoing Aire expression, as suggested previously (9). Thus, the unique properties of post-Aire mTECs in establishing self-tolerance need to be investigated further.

Finally, we found that the increased proportions of $CD80^{high}$ mTECs in Aire-deficient mice were absent on a Rag2-deficient background. The results may suggest that thymocytes (at stages later than double-negative 4), under physiological conditions, provide certain undefined signals that make AEL-mTECs dependent on Aire for their full maturation program. Alternatively, Aire-dependent thymocyte development, as exemplified by the reduced numbers of terminally differentiated single-positive thymocytes in Aire-deficient mice on a Rag2-sufficient background (23), may in turn affect the differentiation program of AEL-mTECs. Thus, some of the unique features of mTECs in Aire-deficient mice are not mTEC autonomous, but cross-talk with mature thymocytes is required for the Aire-dependent differentiation program of AEL-mTECs.

Acknowledgments

We thank Drs. Jun-ichi Miyazaki and Hiroshi Kawamoto for CAG-CAT-EGFP mice and Dr. Shohei Hori for tdRFP mice.

Disclosures

The authors have no financial conflicts of interest.

References

1. Mathis, D., and C. Benoist. 2009. Aire. *Annu. Rev. Immunol.* 27: 287–312.
2. Anderson, M. S., E. S. Venanzi, L. Klein, Z. Chen, S. P. Berzins, S. J. Turley, H. von Boehmer, R. Bronson, A. Dierich, C. Benoist, and D. Mathis. 2002. Projection of an immunological self shadow within the thymus by the aire protein. *Science* 298: 1395–1401.
3. Abramson, J., M. Giraud, C. Benoist, and D. Mathis. 2010. Aire's partners in the molecular control of immunological tolerance. *Cell* 140: 123–135.
4. Oven, I., N. Brdicková, J. Kohoutek, T. Vaupotic, M. Narat, and B. M. Peterlin. 2007. AIRE recruits P-TEFb for transcriptional elongation of target genes in medullary thymic epithelial cells. *Mol. Cell. Biol.* 27: 8815–8823.
5. Org, T., F. Chignola, C. Hetényi, M. Gaetani, A. Rebane, I. Liiv, U. Maran, L. Mollica, M. J. Bottomley, G. Musco, and P. Peterson. 2008. The autoimmune regulator PHD finger binds to non-methylated histone H3K4 to activate gene expression. *EMBO Rep.* 9: 370–376.
6. Matsumoto, M. 2011. Contrasting models for the roles of Aire in the differentiation program of epithelial cells in the thymic medulla. *Eur. J. Immunol.* 41: 12–17.
7. Gillard, G. O., J. Dooley, M. Erickson, L. Peltonen, and A. G. Farr. 2007. Aire-dependent alterations in medullary thymic epithelium indicate a role for Aire in thymic epithelial differentiation. *J. Immunol.* 178: 3007–3015.
8. Yano, M., N. Kuroda, H. Han, M. Meguro-Horike, Y. Nishikawa, H. Kiyonari, K. Maemura, Y. Yanagawa, K. Obata, S. Takahashi, et al. 2008. Aire controls the differentiation program of thymic epithelial cells in the medulla for the establishment of self-tolerance. *J. Exp. Med.* 205: 2827–2838.
9. Wang, X., M. Laan, R. Bichele, K. Kisand, H. S. Scott, and P. Peterson. 2012. Post-Aire maturation of thymic medullary epithelial cells involves selective expression of keratinocyte-specific autoantigens. *Front. Immunol.* 3: 19.
10. Gray, D., J. Abramson, C. Benoist, and D. Mathis. 2007. Proliferative arrest and rapid turnover of thymic epithelial cells expressing Aire. *J. Exp. Med.* 204: 2521–2528.
11. Hubert, F. X., S. A. Kinkel, P. E. Crewther, P. Z. Cannon, K. E. Webster, M. Link, R. Uibo, M. K. O'Bryan, A. Meager, S. P. Forehan, et al. 2009. Aire-deficient C57BL/6 mice mimicking the common human 13-base pair deletion mutation present with only a mild autoimmune phenotype. *J. Immunol.* 182: 3902–3918.
12. Kuroda, N., T. Mitani, N. Takeda, N. Ishimaru, R. Arakaki, Y. Hayashi, Y. Bando, K. Izumi, T. Takahashi, T. Nomura, et al. 2005. Development of autoimmunity against transcriptionally unrepressed target antigen in the thymus of Aire-deficient mice. *J. Immunol.* 174: 1862–1870.
13. Anderson, G., P. J. Lane, and E. J. Jenkinson. 2007. Generating intrathymic microenvironments to establish T-cell tolerance. *Nat. Rev. Immunol.* 7: 954–963.
14. Kyewski, B., and J. Derbinski. 2004. Self-representation in the thymus: an extended view. *Nat. Rev. Immunol.* 4: 688–698.
15. Nishikawa, Y., F. Hirota, M. Yano, H. Kitajima, J. Miyazaki, H. Kawamoto, Y. Mouri, and M. Matsumoto. 2010. Biphasic Aire expression in early embryos and in medullary thymic epithelial cells before end-stage terminal differentiation. *J. Exp. Med.* 207: 963–971.
16. Dooley, J., M. Erickson, and A. G. Farr. 2008. Alterations of the medullary epithelial compartment in the Aire-deficient thymus: implications for programs of thymic epithelial differentiation. *J. Immunol.* 181: 5225–5232.
17. Feil, R., J. Wagner, D. Metzger, and P. Chambon. 1997. Regulation of Cre recombinase activity by mutated estrogen receptor ligand-binding domains. *Biochem. Biophys. Res. Commun.* 237: 752–757.
18. Kawamoto, S., H. Niwa, F. Tashiro, S. Sano, G. Kondoh, J. Takeda, K. Tabayashi, and J. Miyazaki. 2000. A novel reporter mouse strain that expresses enhanced green fluorescent protein upon Cre-mediated recombination. *FEBS Lett.* 470: 263–268.
19. Luche, H., O. Weber, T. Nageswara Rao, C. Blum, and H. J. Fehling. 2007. Faithful activation of an extra-bright red fluorescent protein in "knock-in" Cre-reporter mice ideally suited for lineage tracing studies. *Eur. J. Immunol.* 37: 43–53.
20. Guerau-de-Arellano, M., M. Martinic, C. Benoist, and D. Mathis. 2009. Neonatal tolerance revisited: a perinatal window for Aire control of autoimmunity. *J. Exp. Med.* 206: 1245–1252.
21. Metzger, T. C., I. S. Khan, J. M. Gardner, M. L. Mouchess, K. P. Johannes, A. K. Krawisz, K. M. Skrzypczynska, and M. S. Anderson. 2013. Lineage tracing and cell ablation identify a post-aire-expressing thymic epithelial cell population. *Cell Rep.* 5: 166–179.
22. Rossi, S. W., M. Y. Kim, A. Leibbrandt, S. M. Parnell, W. E. Jenkinson, S. H. Glanville, F. M. McConnell, H. S. Scott, J. M. Penninger, E. J. Jenkinson, et al. 2007. RANK signals from $CD4(^{+})3(^{-})$ inducer cells regulate development of Aire-expressing epithelial cells in the thymic medulla. *J. Exp. Med.* 204: 1267–1272.
23. Li, J., Y. Li, J. Y. Yao, R. Jin, M. Z. Zhu, X. P. Qian, J. Zhang, Y. X. Fu, L. Wu, Y. Zhang, and W. F. Chen. 2007. Developmental pathway of $CD4^{+}CD8^{-}$ medullary thymocytes during mouse ontogeny and its defect in $Aire^{-/-}$ mice. *Proc. Natl. Acad. Sci. USA* 104: 18175–18180.

Genetic correction of *HAX1* in induced pluripotent stem cells from a patient with severe congenital neutropenia improves defective granulopoiesis

Tatsuya Morishima,[1] Ken-ichiro Watanabe,[1] Akira Niwa,[2] Hideyo Hirai,[3] Satoshi Saida,[1] Takayuki Tanaka,[2] Itaru Kato,[1] Katsutsugu Umeda,[1] Hidefumi Hiramatsu,[1] Megumu K. Saito,[2] Kousaku Matsubara,[4] Souichi Adachi,[5] Masao Kobayashi,[6] Tatsutoshi Nakahata,[2] and Toshio Heike[1]

[1]Department of Pediatrics, Graduate School of Medicine, Kyoto University, Kyoto; [2]Department of Clinical Application, Center for iPS Cell Research and Application, Kyoto University, Kyoto; [3]Department of Transfusion Medicine and Cell Therapy, Kyoto University Hospital, Kyoto; [4]Department of Pediatrics, Nishi-Kobe Medical Center, Kobe; [5]Human Health Sciences, Graduate School of Medicine, Kyoto University, Kyoto; and [6]Department of Pediatrics, Hiroshima University Graduate School of Biomedical Sciences, Hiroshima, Japan

ABSTRACT

HAX1 was identified as the gene responsible for the autosomal recessive type of severe congenital neutropenia. However, the connection between mutations in the *HAX1* gene and defective granulopoiesis in this disease has remained unclear, mainly due to the lack of a useful experimental model for this disease. In this study, we generated induced pluripotent stem cell lines from a patient presenting for severe congenital neutropenia with *HAX1* gene deficiency, and analyzed their *in vitro* neutrophil differentiation potential by using a novel serum- and feeder-free directed differentiation culture system. Cytostaining and flow cytometric analyses of myeloid cells differentiated from patient-derived induced pluripotent stem cells showed arrest at the myeloid progenitor stage and apoptotic predisposition, both of which replicated abnormal granulopoiesis. Moreover, lentiviral transduction of the *HAX1* cDNA into patient-derived induced pluripotent stem cells reversed disease-related abnormal granulopoiesis. This *in vitro* neutrophil differentiation system, which uses patient-derived induced pluripotent stem cells for disease investigation, may serve as a novel experimental model and a platform for high-throughput screening of drugs for various congenital neutrophil disorders in the future.

Introduction

Severe congenital neutropenia (SCN) is a rare myelopoietic disorder resulting in recurrent life-threatening infections due to a lack of mature neutrophils,[1] and individuals with SCN present for myeloid hypoplasia with an arrest of myelopoiesis at the promyelocyte/myelocyte stage.[1,2] SCN is actually a multigene syndrome that can be caused by inherited mutations in several genes. For instance, approximately 60% of SCN patients are known to carry autosomal dominant mutations in the *ELANE* gene, which encodes neutrophil elastase (NE).[3] An autosomal recessive type of SCN was first described by Kostmann in 1956,[4] and defined as Kostmann disease. Although the gene responsible for this classical type of SCN remained unknown for more than 50 years, Klein *et al.* identified mutations in *HAX1* to be responsible for this type of SCN in 2007.[5] HAX1 localizes predominantly to mitochondria, where it controls inner mitochondrial membrane potential ($\Delta\psi_m$) and apoptosis.[6,7] Although an increase in apoptosis in mature neutrophils was presumed to cause neutropenia in HAX1 gene deficiency,[5] the connection between *HAX1* gene mutations and defective granulopoiesis in SCN has remained unclear.

To control infections, SCN patients are generally treated with granulocyte colony-stimulating factor (G-CSF); however, long-term G-CSF therapy associates with an increased risk of myelodysplastic syndrome and acute myeloid leukemia (MDS/AML).[8,9] Although hematopoietic stem cell transplantations are available as the only curative therapy for this disease, they can result in various complications and mortality.[4]

Many murine models of human congenital and acquired diseases are invaluable for disease investigation as well as for novel drug discoveries. However, their use in a research setting can be limited if they fail to mimic strictly the phenotype of the human disease in question. For instance, the *Hax1* knock-out mouse is characterized by lymphocyte loss and neuronal apoptosis, but not neutropenia.[10] Thus, it is not a suitable experimental model for SCN. Induced pluripotent stem (iPS) cells are reprogrammed somatic cells with embryonic stem (ES) cell-like characteristics produced by the introduction of specific transcription factors,[11,16] and they may substitute murine models of human disease. It is believed that iPS cell technology, which generates disease-specific pluripotent stem cells in combination with directed cell differentiation, will contribute enormously to patient-oriented research, including disease pathophysiology, drug screening, cell transplantation, and gene therapy.

In vitro neutrophil differentiation systems, which can reproduce the differentiation of myeloid progenitor cells to mature neutrophils, are needed to understand the pathogenesis of SCN better. Recently, we established a neutrophil differentia-

 doi:10.3324/haematol.2013.083873
The online version of this article has a Supplementary Appendix.
Manuscript received on January 9, 2013. Manuscript accepted on August 20, 2013.
Correspondence: heike@kuhp.kyoto-u.ac.jp

tion system from human iPS cells[17] as well as a serum- and feeder-free monolayer hematopoietic culture system from human ES and iPS cells.[18] In this study, we generate iPS cell lines from an SCN patient with *HAX1* gene deficiency and differentiate them into neutrophils *in vitro*. Furthermore, we corrected for the *HAX1* gene deficiency in HAX1-iPS cells by lentiviral transduction with *HAX1* cDNA and analyzed the neutrophil differentiation potential of these cells. Thus, this *in vitro* neutrophil differentiation system from patient-derived iPS cells may be a useful model for future studies in SCN patients with *HAX1* gene deficiency.

Methods

Human iPS cell generation

Skin biopsy specimens were obtained from an 11-year old male SCN patient with *HAX1* gene deficiency.[19] This study was approved by the Ethics Committee of Kyoto University, and informed consent was obtained from the patient's guardians in accordance with the Declaration of Helsinki. Fibroblasts were expanded in DMEM (Nacalai Tesque, Inc., Kyoto, Japan) containing 10% FBS (vol/vol, Invitrogen, Carlsbad, CA, USA) and 0.5% penicillin and streptomycin (wt/vol, Invitrogen). Generation of iPS cells was performed as described previously.[12] In brief, we introduced *OCT3/4, SOX2, KLF4*, and *cMYC* using ecotropic retroviral transduction into patient's fibroblasts expressing mouse *Slc7a1*. Six days after transduction, cells were harvested and re-plated onto mitotically inactive SNL feeder cells. On the following day, DMEM was replaced with primate ES cell medium (ReproCELL, Kanagawa, Japan) supplemented with basic fibroblast growth factor (5 ng/mL, R&D Systems, Minneapolis, MN, USA). Three weeks later, individual colonies were isolated and expanded.

Maintenance of cells

Control ES (KhES-1) and control iPS (253G4 and 201B6) cells were kindly provided by Drs. Norio Nakatsuji and Shinya Yamanaka (Kyoto University, Kyoto, Japan), respectively. These human ES and iPS cell lines were maintained on mitomycin-C (Kyowa Hakko Kirin, Tokyo, Japan)-treated SNL feeder cells as described previously[17] and subcultured onto new SNL feeder cells every seven days.

Flow cytometric analysis

Cells were stained with antibodies as reported previously.[17] Samples were analyzed using an LSR flow cytometer and Cell Quest software (Becton-Dickinson).

Neutrophil differentiation of iPS cells

In a previous study, we established a serum and feeder-free monolayer hematopoietic culture system from human ES and iPS cells.[18] In this study, we modified this culture system to direct neutrophil differentiation. iPS cell colonies were cultured on growth factor-reduced Matrigel (Becton-Dickinson)-coated cell culture dishes in Stemline II hematopoietic stem cell expansion medium (Sigma-Aldrich, St. Louis, MO, USA) containing the insulin-transferrin-selenium (ITS) supplement (Invitrogen) and cytokines. iPS cells were treated with cytokines as follows: bone morphogenetic protein (BMP) 4 (20 ng/mL, R&D Systems) was added for four days and then replaced with vascular endothelial growth factor (VEGF) 165 (40 ng/mL, R&D Systems) on Day 4. On Day 6, VEGF 165 was replaced with a combination of stem cell factor (SCF, 50 ng/mL, R&D Systems), interleukin (IL)-3 (50 ng/mL, R&D Systems), thrombopoietin (TPO, 5 ng/mL, kindly provided by Kyowa Hakko Kirin), and G-CSF (50 ng/mL, also kindly provided by Kyowa Hakko Kirin). Thereafter, medium was replaced every five days.

Dead cell removal and CD45$^+$ leukocyte separation

Floating cells were collected, followed by the removal of dead cells and cellular debris with the Dead Cell Removal kit (Miltenyi Biotec, Bergisch Gladbach, Germany). CD45$^+$ cells were then separated using human CD45 microbeads (Miltenyi Biotec). Cell separation procedures were performed using the autoMACS Pro Separator (Miltenyi Biotec).

Statistical analysis

Statistical analysis was carried out using Student's t-test. $P<0.05$ was considered statistically significant.

Results

Generation of iPS cell lines from an SCN patient with HAX1 gene deficiency

To generate patient-derived iPS cell lines, dermal fibroblasts were obtained from a male SCN patient with a homozygous 256C-to-T transition resulting in an R86X mutation in the *HAX1* gene.[19] These fibroblasts were reprogrammed to iPS cells after transduction with retroviral vectors encoding *OCT3/4, SOX2, KLF4* and *cMYC*,[12] and a total of 11 iPS cell clones were obtained. From these, we randomly selected three clones for propagation and subsequent analyses. One of these clones (HAX1 4F5) was generated with four factors (*OCT3/4, SOX2, KLF4*, and *cMYC*); the remaining clones (HAX1 3F3 and 3F5) were generated with three factors (*OCT3/4, SOX2*, and *KLF4*).[12]

All of these patient-derived iPS cell clones showed a characteristic human ES cell-like morphology (Figure 1A), and they propagated for serial passages in human ES cell maintenance culture medium. Quantitative PCR analysis showed the expression of *NANOG*, a pluripotent marker gene, to be comparable to that of control ES (KhES-1) and iPS (253G4 and 201B6) cells (Figure 1B). Surface marker analysis indicated that they were also positive for SSEA4, a human ES and iPS cell marker (Figure 1C). DNA sequencing analysis verified an identical mutation in the *HAX1* gene in all established iPS cell clones (Figure 1D). The pluripotency of all iPS cell clones was confirmed by the presence of cell derivatives representing all three germ layers by teratoma formation after subcutaneous injection of undifferentiated iPS cells into immunocompromised NOD/SCID/γc^{null} mice (Figure 1E).

To validate the authenticity of iPS cells further, we investigated the expression of the four genes that were used for iPS cell generation. The expression level of all endogenous genes was comparable to control ES and iPS cells. On the other hand, transgene expression was largely undetectable in patient-derived iPS cell clones (*Online Supplementary Figure S1A*). Chromosomal analysis revealed that all patient-derived iPS cell clones maintained a normal karyotype (*Online Supplementary Figure S1B*). Genetic identity was shown by short tandem repeat analysis (*Online Supplementary Figure S1C*).

Taken collectively, these results indicate that iPS cell clones were comprised of good quality iPS cells derived from the somatic cells of an SCN patient with *HAX1* gene deficiency (HAX1-iPS cells).

Maturation arrest at the progenitor level in neutrophil differentiation from HAX1-iPS cells

The paucity of mature neutrophils in the peripheral blood and a maturation arrest at the promyelocyte/myelocyte stage in the bone marrow are characteristic laboratory findings presented in the SCN patients with *HAX1* gene deficiency. To investigate whether our patient-derived iPS cell model accurately replicated this disease phenotype, we assessed neutrophil differentiation from HAX1-iPS cells by using a serum- and feeder-free monolayer culture system[18] with minor modifications (Online *Supplementary Figure S2*).

In this system, we cultured iPS cell colonies on Matrigel-coated dishes in serum-free medium supplemented with several cytokines and obtained hematopoietic cells as floating cells on approximately Day 26 of differentiation. May-Giemsa staining of floating live CD45$^+$ cells derived from normal iPS cells showed that approximately 40% were mature neutrophils (Figure 2A and B). The remaining cells consisted of immature myeloid cells as well as a small number of macrophages. Cells of other lineages such as erythroid or lymphoid cells were not observed. On the other hand, HAX1-iPS cell-derived blood cells contained only approximately 10% mature neutrophils and approxi-

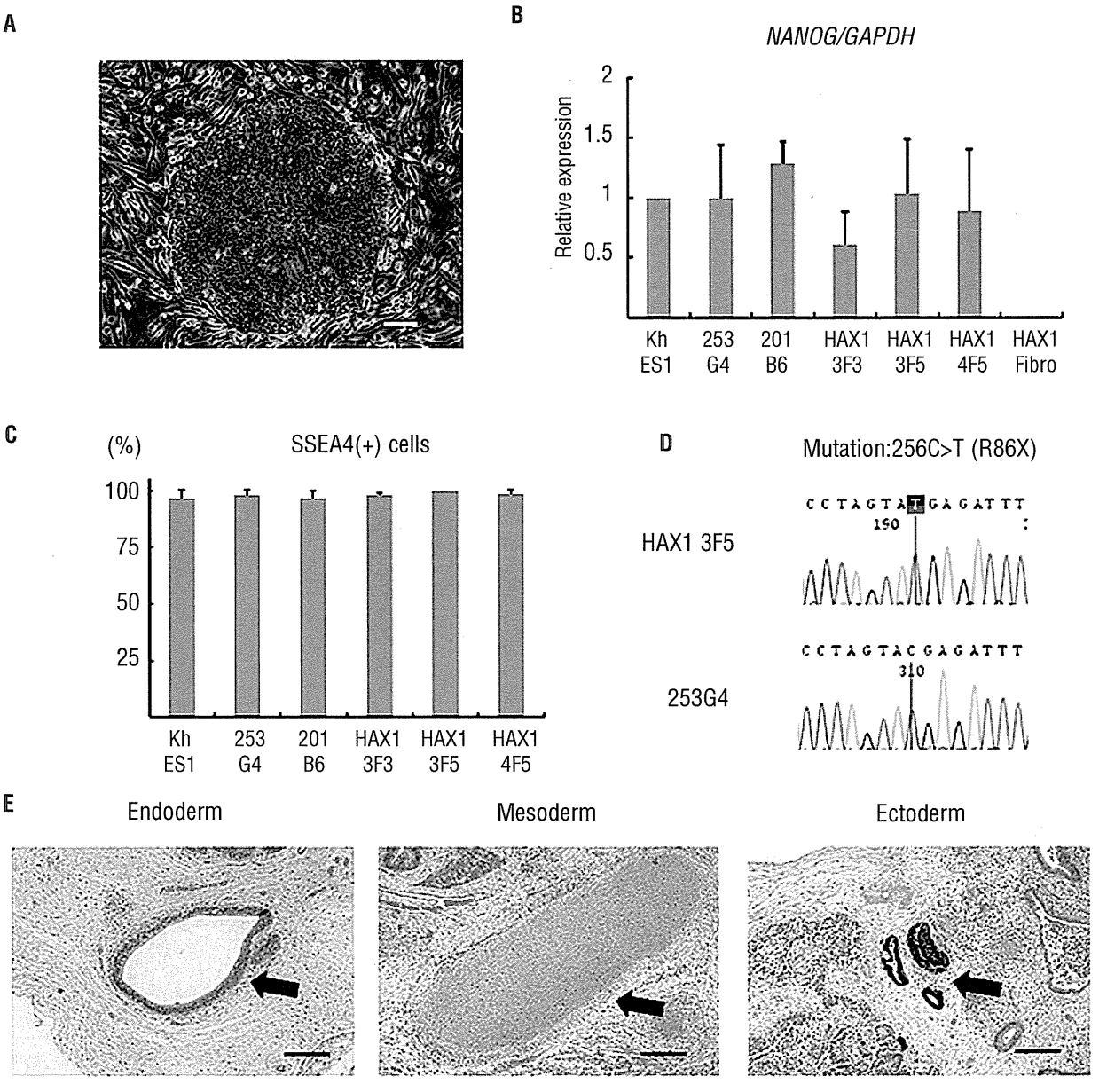

Figure 1. Generation of iPS cell lines from an SCN patient with *HAX1* gene deficiency. (A) Human ES cell-like morphology of HAX1-iPS cells. Scale bar: 200 μm. (B) *NANOG* expression in HAX1-iPS cells, control iPS cells (253G4 and 201B6), and patient-derived fibroblasts (HAX1 Fibro) compared to control ES cells (KhES1). *GAPDH* was used as an internal control (n = 3; bars represent SDs). (C) SSEA-4 expression analysis using flow cytometry. Gated on TRA1-85$^+$DAPI$^-$ cells as viable human iPS (ES) cells (n = 3; bars represent SDs). (D) DNA sequencing analysis of the *HAX1* gene in iPS cells. HAX1-iPS cells showed 256C>T (R86X) mutation that was found in the patient. (E) Teratoma formation from HAX1-iPS cells in the NOD/SCID/γc^{null} (NOG) mouse. Arrows indicate the following; Endoderm: respiratory epithelium; Mesoderm: cartilage; Ectoderm: pigmented epithelium. Scale bars: 200 μm. (A, D-E) Representative data (HAX1 3F5) are shown.

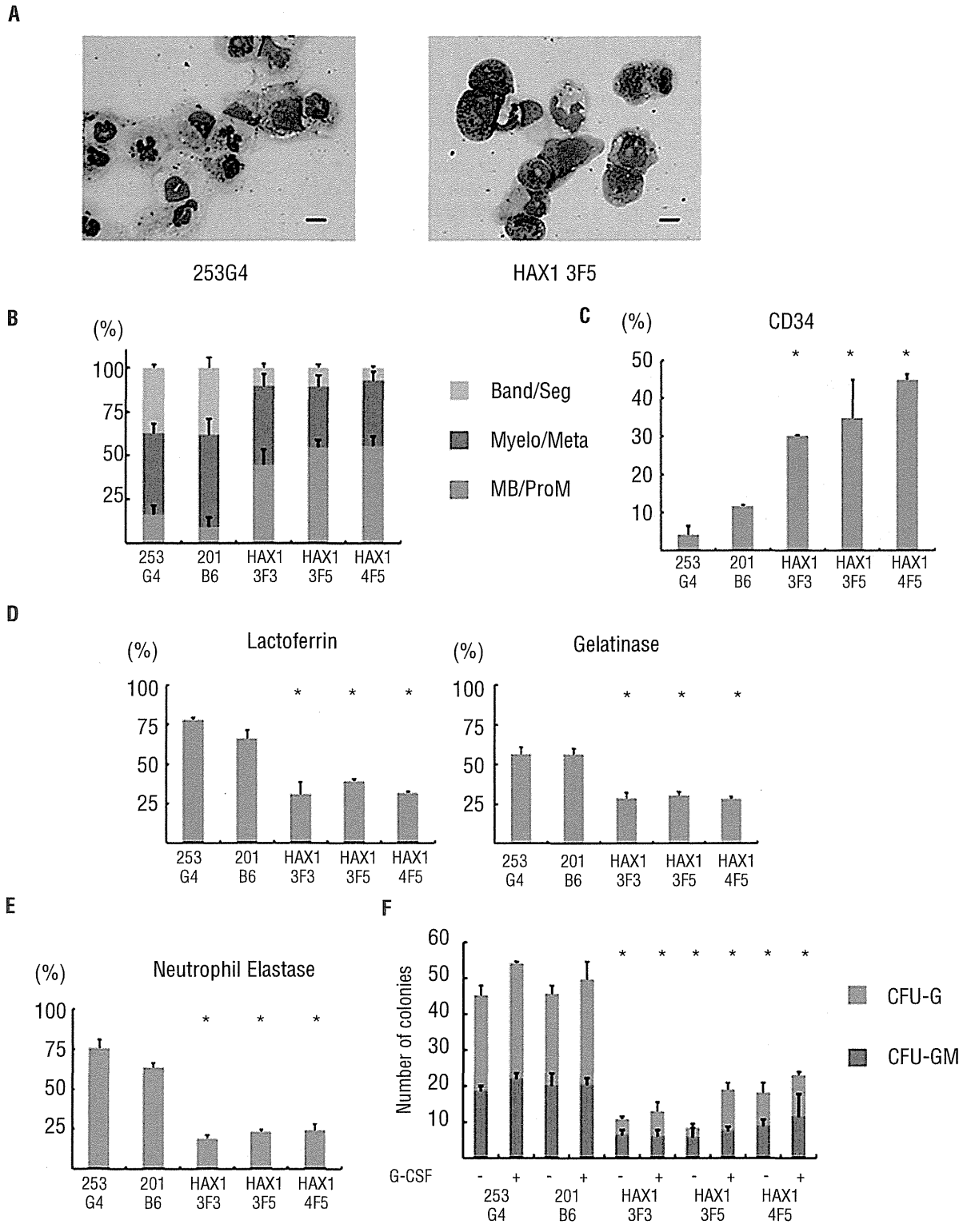

Figure 2. Maturation arrest at the progenitor level in neutrophil differentiation from HAX1-iPS cells. (A) May-Giemsa staining of CD45$^+$ cells derived from normal (253G4) and HAX1-iPS (HAX1 3F5) cells. Scale bars: 10 μm. (B) Morphological classification of CD45$^+$ cells derived from iPS cells. Cells were classified into three groups: myeloblast and promyelocyte (MB/ProM), myelocyte and metamyelocyte (Myelo/Meta), and band and segmented neutrophils (Band/Seg) (n = 3; bars represent SDs). (C) Flow cytometric analysis of CD45$^+$ cells derived from iPS cells. Cells gated on human CD45$^+$ DAPI$^-$ were analyzed (n = 3; bars represent SDs; *P<0.05 compared to control iPS cells). (D) Immunocytochemical analysis of CD45$^+$ cells derived from iPS cells (n = 3; bars represent SDs; *P<0.05 compared to control iPS cells). (E) NE staining of CD45$^+$ cells derived from iPS cells (n = 3; bars represent SDs; *P<0.05 compared to control iPS cells). (F) Colony-forming assay of cells derived from iPS cells. On Day 16, living adherent cells were collected and cultured in methylcellulose medium (see *Online Supplementary Appendix*). The number of colonies generated from 1×10^4 cells is indicated (n = 3; bars represent SD; *P<0.05 compared to control iPS cells). (A–E) Live CD45$^+$ cells derived from normal and HAX1-iPS cells on Day 26 of neutrophil differentiation were analyzed. Dead cells and CD45$^-$ cells were depleted using an autoMACS Pro separator (see *Methods*).

mately 50% immature myeloid cells, including myeloblasts and promyelocytes (Figure 2A and B). Flow cytometric analysis revealed that the percentage of $CD34^+$ cells within HAX1-iPS cell-derived blood cells was significantly higher than in normal iPS cell-derived blood cells (Figure 2C), which also showed that the percentage of phenotypically immature myeloid cells was higher in HAX1-iPS cell-derived blood cells than in normal iPS cell-derived blood cells.

Immunocytochemical analysis for lactoferrin and gelatinase, which are constitutive proteins of neutrophil specific granules observed in mature neutrophils, showed that the proportion of these granule-positive cells was significantly lower in HAX1-iPS cell-derived blood cells than in normal iPS cell-derived blood cells (Figure 2D). NE is a protease stored in primary granules of neutrophilic granulocytes that are formed at the promyelocytic phase of granulocyte differentiation. *ELANE* mRNA expression in myeloid progenitors and the protein level of NE in plasma are markedly reduced in SCN patients with mutations in *ELANE* or *HAX1*.[20] Consistent with this, the proportion of NE-positive cells was significantly lower in blood cells derived from HAX1-iPS cells than in those derived from normal iPS cells (Figure 2E). Thus, the level of functionally mature neutrophils decreased during *in vitro* granulopoietic differentiation of HAX1-iPS cells.

Next, we analyzed the colony-forming potential of HAX1-iPS cell-derived myeloprogenitor cells. Significantly fewer colonies, which were classified as granulocyte-macrophage (GM) or granulocyte (G) colony-forming units (CFU), were derived from HAX1-iPS cells than from control iPS cells. Furthermore, the colonies derived from HAX1-iPS cells were predominantly CFU-GM (Figure 2F). Thus, maturation arrest occurred at the clonogenic progenitor stage during *in vitro* neutrophil differentiation of HAX1-iPS cells.

SCN is characterized by severe neutropenia with very low absolute neutrophil counts in peripheral blood, and many SCN patients respond to G-CSF treatment.[1,2] In colony-forming assays using bone marrow cells of SCN patients, primitive myeloid progenitor cells have reduced responsiveness to hematopoietic cytokines including G-CSF.[21,22] Therefore, we next examined the response of HAX1-iPS cell-derived blood cells to G-CSF using a colony-forming assay. Although the number of colonies derived from HAX1-iPS cells slightly increased following the addition of G-CSF, it remained significantly lower than the number of colonies derived from control iPS cells in the absence of G-CSF (Figure 2F). These results indicate that the responsiveness of HAX1-iPS-derived blood cells to G-CSF was insufficient to restore the neutrophil count to a normal level and are consistent with the fact that the absolute neutrophil counts of SCN patients remain low following G-CSF therapy.[19,21]

Neutrophils derived from HAX1-iPS cells are predisposed to undergo apoptosis due to their reduced $\Delta\psi_m$

Previous studies have shown HAX1 to localize to mitochondria[6] and to mediate anti-apoptotic activity.[7] Interestingly, this apoptotic predisposition of neutrophils due to their reduced $\Delta\psi_m$ was observed in HAX1-deficient patients,[5] prompting us to examine apoptosis in HAX1-iPS cell-derived blood cells. Consistent with these reports, HAX1-iPS cell-derived blood cells showed a significantly higher percentage of Annexin V-positive cells than in control cells (Figure 3A). In addition, a mitochondrial membrane potential assay revealed that the percentage of cells with a low $\Delta\psi_m$ was significantly higher in HAX1-iPS cell-derived blood cells than in blood cells derived from control iPS cells (Figure 3B). By contrast, the percentage of cells with a low $\Delta\psi_m$ was similar in undifferentiated HAX1-iPS cells and undifferentiated control iPS cells (*Online Supplementary Figure S3*).

Thus, increased apoptosis due to reduced $\Delta\psi_m$ causes defective granulopoiesis during neutrophil differentiation from HAX1-iPS cells, similar to the process observed in SCN patients with *HAX1* gene deficiency.

Lentiviral transduction of HAX1 cDNA improves maturation arrest and apoptotic predisposition of HAX1-iPS cells

Because most *HAX1* gene mutations in SCN patients are nonsense mutations resulting in a premature stop codon and protein truncation,[23] loss of the HAX1 protein is believed to cause severe neutropenia. To uncover the pathophysiological hallmarks of this disease, we performed lentiviral transduction of *HAX1* cDNA into HAX1-iPS cells.

We constructed lentiviral vectors that expressed *HAX1* cDNA and EGFP as a marker gene (pCSII-EF-IEGFP; EGFP

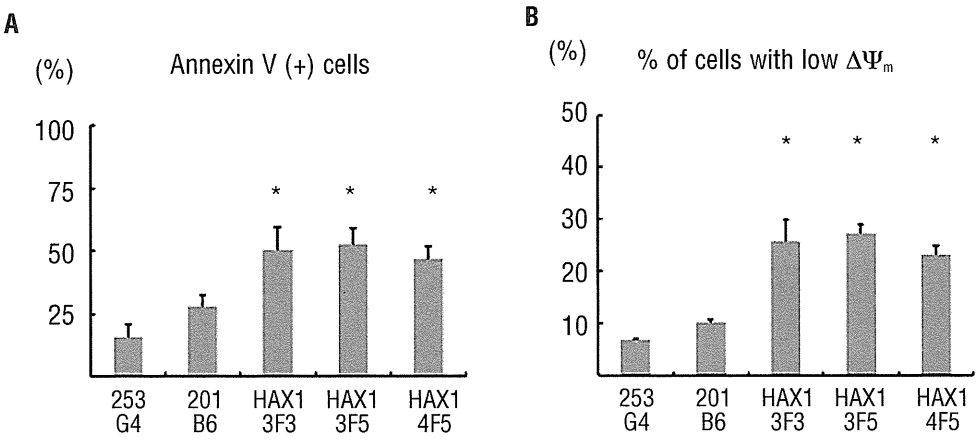

Figure 3. Neutrophils derived from HAX1-iPS cells are predisposed to undergo apoptosis due to their reduced Δψm. Annexin V assay (A) and mitochondrial membrane potential assay (B) of iPS cell-derived cells on Day 26 of neutrophil differentiation using flow cytometry. Cells gated on human $CD45^+$ were analyzed (n = 3; bars represent SDs; *$P<0.05$ to control iPS cells).

only, pCSII-EF-HAX1-IEGFP; HAX1 cDNA and EGFP) (Figure 4A). Efficient transduction of HAX1-iPS cells with these lentiviral vectors (HAX1 3F5+GFP; HAX1 3F5 transduced with pCSII-EF-IEGFP, HAX1 3F5+HAX1; HAX1 3F5 transduced with pCSII-EF-HAX1-IEGFP) was confirmed by a significant increase in HAX1 protein by Western blotting analysis (Figure 4B).

We then differentiated these lentiviral-transduced iPS cells into neutrophils, and examined whether defective granulopoiesis and apoptotic predisposition could be reversed. Morphologically, cells derived from HAX1 3F5+HAX1 showed a higher proportion of mature neutrophils than cells derived from HAX1 3F5+GFP and HAX1 3F5 (Figure 5A and B). Flow cytometric analysis revealed that the proportion of $CD34^+$ cells was significantly lower in the cells derived from HAX1 3F5+HAX1 than HAX1 3F5+GFP and HAX1 3F5 (Figure 5C). Immunocytochemical analysis for lactoferrin and gelatinase showed that the proportion of these granule-positive cells in generated blood cells was significantly higher in HAX 3F5+HAX1 than in HAX13F5+GFP and HAX1 3F5 (Figure 5D). These results indicated that *HAX1* cDNA increased the number of mature neutrophils in the neutrophil differentiation culture from HAX1-iPS cells *in vitro*. In addition, the percentage of NE-positive cells was significantly higher in cells derived from HAX1 3F5+HAX1 than in cells derived from HAX1 3F5+GFP and HAX1 3F5 (Figure 5E). Furthermore, the number of colonies derived from HAX1 3F5+HAX1 was comparable to the number derived from control cells (Figure 5F).

HAX1 3F5+HAX1-derived blood cells showed a significantly lower percentage of Annexin V-positive cells (Figure 6A) and a significantly lower percentage of cells with a low $\Delta\psi_m$ (Figure 6B) than HAX13F5+GFP and HAX1 3F5-derived blood cells. These results indicated that only *HAX1* cDNA transduction improved defective granulopoiesis and apoptotic predisposition due to low $\Delta\psi_m$ in the neutrophil differentiation culture from HAX1-iPS cells *in vitro*.

Discussion

Animal models and *in vitro* cultures consisting of cells derived from patients are often used to investigate disease pathophysiology and to develop novel therapies. Unfortunately, *Hax1* knock-out mice fail to reproduce abnormal granulopoiesis as observed in SCN patients.[10] Moreover, bone marrow cells are not an ideal experimental tool because it is difficult to obtain sufficient blood cells due to the invasiveness of the aspiration procedure. Moreover, the pathophysiological mechanisms occurring during early granulopoiesis are difficult to address in primary patient samples.

Our established culture system efficiently induced directed hematopoietic differentiation, which consisted of myeloid cells at different stages of development, from various control and patient-derived HAX1-iPS cell lines. Furthermore, this *in vitro* neutrophil differentiation system produced sufficient myeloid cells, which enabled us to perform various types of assays. In addition, flow cytom-

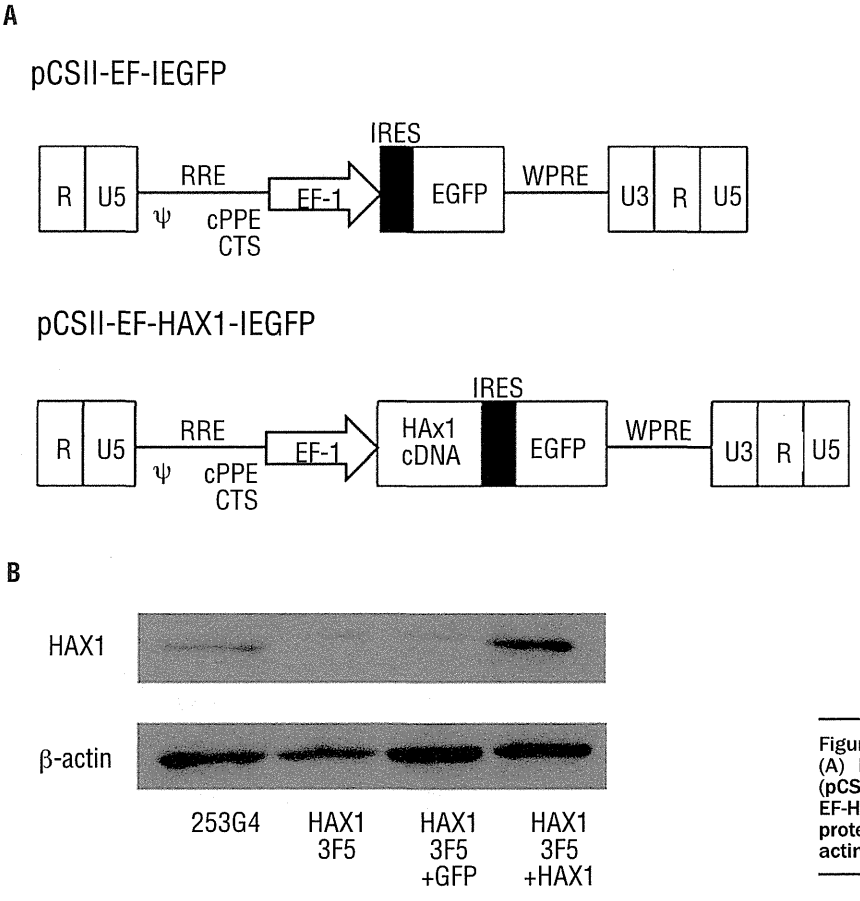

Figure 4. Lentiviral transduction of HAX1-iPS cells. (A) Lentiviral vector constructs with only EGFP (pCSII-EF-IEGFP), and *HAX1* cDNA and EGFP (pCSII-EF-HAX1-IEGFP). (B) Western blot analysis for HAX1 protein in lentivirally-transduced HAX1-iPS cells. β-actin was used as a loading control.

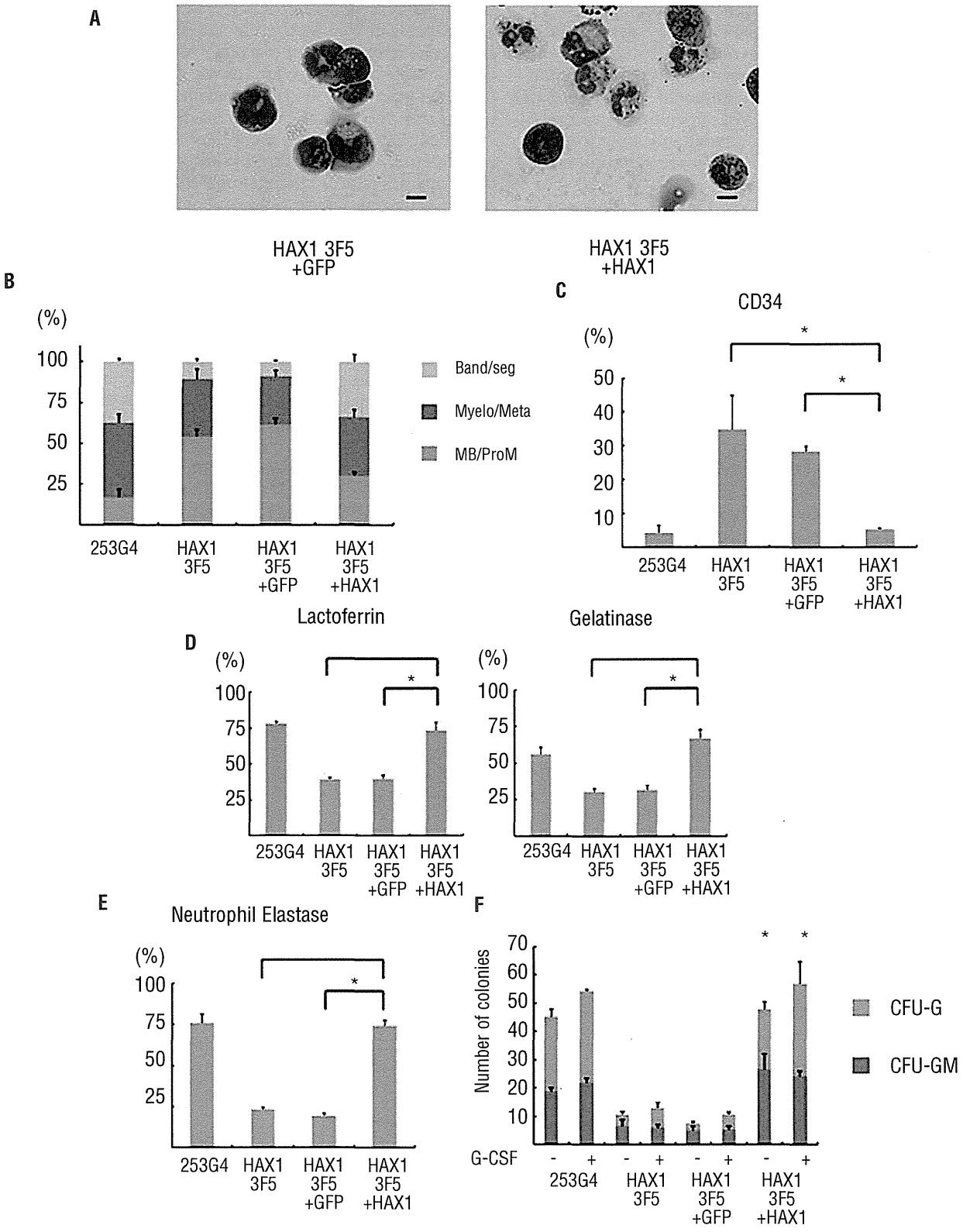

Figure 5. Lentiviral transduction of HAX1 cDNA improves maturation arrest of HAX1-iPS cells. (A) May-Giemsa staining of CD45$^+$ cells derived from HAX1 3F5+GFP and HAX1 3F5+HAX1 cells. Scale bars: 10 μm. (B) Morphological classification of CD45$^+$ cells derived from lentivirally-transduced iPS cells. (n = 3; bars represent SDs). (C) Flow cytometric analysis of CD45$^+$ cells derived from lentivirally-transduced iPS cells. Cells gated on GFP$^+$ human CD45$^+$ DAPI$^-$ were analyzed (n = 3; bars represent SDs; *P<0.05). (D) Immunocytochemical analysis of CD45$^+$ cells derived from lentivirally-transduced iPS cells (n = 3; bars represent SDs; *P<0.05). (E) NE staining of CD45$^+$ cells derived from lentivirally-transduced iPS cells (n = 3; bars represent SDs; *P<0.05). (F) Colony-forming assay of lentivirally-transduced cells derived from iPS cells. The number of colonies derived from 1×10^4 cells is indicated (n = 3; bars represent SD; *P<0.05 compared to HAX1 3F5 and HAX1 3F5+GFP). (A-E) Live CD45$^+$ cells derived from lentivirally-transduced iPS cells on Day 26 of neutrophil differentiation were analyzed. Dead cells and CD45- cells were depleted using an autoMACS Pro separator (see *Methods*).

etry, a colony-forming assay, and cytostaining of HAX1-iPS cell-derived blood cells quantitatively demonstrated maturation arrest at the progenitor level and apoptotic predisposition due to low $\Delta\psi_m$ resulting in defective granulopoiesis, which were typically observed in SCN patients with *HAX1* gene deficiency. Thus, our culture system may serve as a novel experimental model and a platform for high-throughput screening of drugs for neutropenia in SCN with *HAX1* gene deficiency.

A colony-forming assay showed that the response to G-CSF administration correlated well with the responsiveness of SCN patients to G-CSF therapy. Defective granulopoiesis was recently reported in SCN-iPS cells with a mutation in *ELANE*.[24] Our data showing defective granulopoiesis and reduced response to G-CSF administration are generally consistent with this report. The slight differences in CFU-G/GM colony-forming potential between this previous study and the current study might be due to differences in the causative gene (*HAX1* or *ELANE*) or the culture system used for neutrophil differentiation, and/or to variation in the differentiation capabilities of the clones.

In our serum and feeder-free monolayer culture system, human ES and iPS cells differentiate into hematopoietic and endothelial cells via common KDR^+CD34^+ hemoangiogenic progenitors, which exist during early embryogenesis.[18] Therefore, emergence of abnormal granulopoiesis in this system suggests that disease onset might occur at early hematopoietic stage (yolk sac or fetal liver), which would have never been addressed with patient samples.

We also showed that *HAX1* cDNA transduction could reverse disease-related phenotypes such as abnormal granulopoiesis and apoptotic predisposition. Although little is known about the pathophysiology of SCN with *HAX1* gene deficiency, these results clearly indicated that a loss in HAX1 protein might be the primary cause of neutropenia. These results also indicated the possibility of using patient-derived iPS cells for gene therapy; however, there are technical difficulties that would preclude these cells from being used in a clinical setting. Lentiviral vectors that randomly integrate transgenes can affect the expression of related genes, including cancer-related genes.[25-28] To overcome these problems, we are required to select clones in which transgenes are integrated 'safe harbor' sites and highly expressed without perturbation of neighboring gene expression,[29] or to take the zinc finger nuclease-mediated gene targeting approach[30-32] specifically to a predesigned safe harbor site such as the *AAVS1* locus,[33] which has previously been shown to permit stable expression of transgenes with minimal effects on nearby genes.

The pluripotency of patient-derived iPS cells enables investigation of the pathophysiology of various organ abnormalities and/or dysfunctions. Many types of inherited bone marrow failure syndrome were characterized by multisystem developmental defects that affected the heart, kidney, skeletomuscular system, and central nervous system. Among these, neurological symptoms were frequently seen in SCN patients with *HAX1* gene deficiency,[19,23,34] suggesting that a loss in HAX1 may also affect neural development. Indeed, our patient also presented for epilepsy and severe delays in motor, cognitive, and intellectual development.[19] In patient-derived cells, $\Delta\psi_m$ was not reduced in undifferentiated iPS cells but was reduced in differentiated neutrophils. No marked abnormalities in teratoma formation by HAX1-iPS cells were observed. These results are partially consistent with the fact that SCN patients with a *HAX1* gene deficiency have only neutropenia and neurological symptoms, despite *HAX1* being a ubiquitously expressed gene.[6] Because some of these neurological symptoms cannot be reproduced in the currently available mouse model,[10] additional studies will be necessary to address the effects of *HAX1* on neural development by directed culture models of patient-derived iPS cells.

In conclusion, patient-derived iPS cell-derived myeloid cells were similar in disease presentation to SCN patients with *HAX1* gene deficiency, which could be reversed by gene correction in a novel *in vitro* neutrophil differentiation system. This culture system will serve as a new tool to facilitate disease modeling and drug screening for congenital neutrophil disorders.

Acknowledgments

The authors would like to thank Dr. Norio Nakatsuji for providing the human ES cell line KhES-1, Dr. Shinya Yamanaka for providing human iPS cell lines 201B6 and 253G4, and Dr. Hiroyuki Miyoshi for providing pCSII-EF-MCS. We are grate-

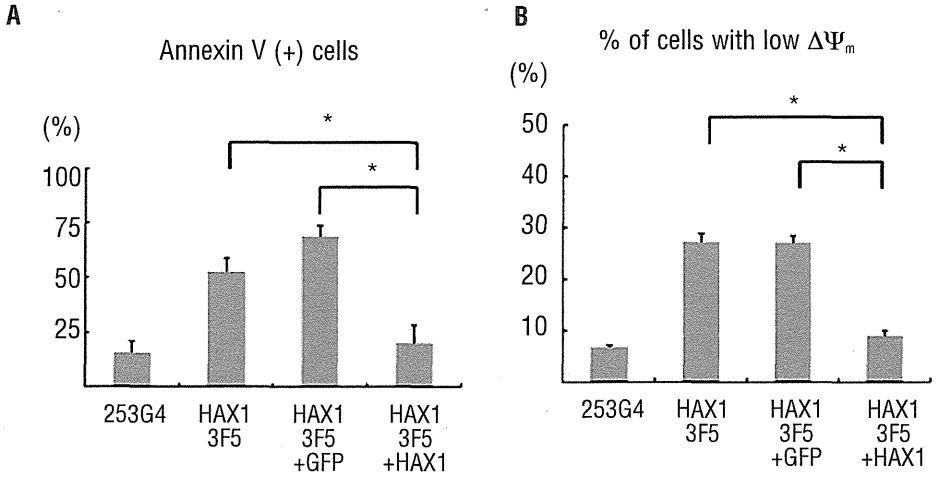

Figure 6. Lentiviral transduction of *HAX1* cDNA prevents HAX1-iPS cells being predisposed to undergo apoptosis. Annexin V assay (A) and mitochondrial membrane potential assay (B) of lentivirally-transduced iPS cell-derived cells on Day 26 of neutrophil differentiation. Cells gated on GFP^+ human $CD45^+$ were analyzed (n = 3; bars represent SDs; *P<0.05).

ful to Kyowa Hakko Kirin for providing TPO and G-CSF. We also thank the Center for Anatomical Studies, Kyoto University Graduate School of Medicine, for immunocytochemical analysis. Funding was provided by grants from the Ministry of Health, Labour and Welfare to KW, TN, and TH, a grant from the Ministry of Education, Culture, Sports, Science and Technology (MEXT) to KW, TN, and TH, grants from the Leading Project of MEXT to TN, a grant from Funding Program for World-Leading Innovative Research and Development on Science and Technology (FIRST Program) of Japan Society for the Promotion of Science (JSPS) to TN, grants from the SENSHIN Medical Research Foundation to IK, and grants from the Fujiwara Memorial Foundation to TM. This work was also supported by the Global COE Program "Center for Frontier Medicine" from MEXT, Japan.

Authorship and Disclosures

Information on authorship, contributions, and financial & other disclosures was provided by the authors and is available with the online version of this article at www.haematologica.org.

References

1. Welte K, Zeidler C, Dale DC. Severe congenital neutropenia. Semin Hematol. 2006;43(3):189-95.
2. Skokowa J, Germeshausen M, Zeidler C, Welte K. Severe congenital neutropenia: inheritance and pathophysiology. Curr Opin Hematol. 2007;14(1):22-8.
3. Dale DC, Person RE, Bolyard AA, Aprikyan AG, Bos C, Bonilla MA, et al. Mutations in the gene encoding neutrophil elastase in congenital and cyclic neutropenia. Blood. 2000;96(7):2317-22.
4. Kostmann R. Infantile genetic agranulocytosis; agranulocytosis infantilis hereditaria. Acta Paediatr Suppl. 1956;45(Suppl 105):1-78.
5. Klein C, Grudzien M, Appaswamy G, Germeshausen M, Sandrock I, Schaffer AA, et al. HAX1 deficiency causes autosomal recessive severe congenital neutropenia (Kostmann disease). Nat Genet. 2007;39 (1):86-92.
6. Suzuki Y, Demoliere C, Kitamura D, Takeshita H, Deuschle U, Watanabe T. HAX-1, a novel intracellular protein, localized on mitochondria, directly associates with HS1, a substrate of Src family tyrosine kinases. J Immunol. 1997;158(6):2736-44.
7. Sharp TV, Wang HW, Koumi A, Hollyman D, Endo Y, Ye H, et al. K15 protein of Kaposi's sarcoma-associated herpesvirus is latently expressed and binds to HAX-1, a protein with antiapoptotic function. J Virol. 2002;76(2):802-16.
8. Freedman MH, Bonilla MA, Fier C, Bolyard AA, Scarlata D, Boxer LA, et al. Myelodysplasia syndrome and acute myeloid leukemia in patients with congenital neutropenia receiving G-CSF therapy. Blood. 2000;96(2):429-36.
9. Rosenberg PS, Zeidler C, Bolyard AA, Alter BP, Bonilla MA, Boxer LA, et al. Stable long-term risk of leukaemia in patients with severe congenital neutropenia maintained on G-CSF therapy. Br J Haematol. 2010;150(2):196-9.
10. Chao JR, Parganas E, Boyd K, Hong CY, Opferman JT, Ihle JN. Hax1-mediated processing of HtrA2 by Parl allows survival of lymphocytes and neurons. Nature. 2008;452(7183):98-102.
11. Takahashi K, Yamanaka S. Induction of pluripotent stem cells from mouse embryonic and adult fibroblast cultures by defined factors. Cell. 2006;126(4):663-76.
12. Takahashi K, Tanabe K, Ohnuki M, Narita M, Ichisaka T, Tomoda K, et al. Induction of pluripotent stem cells from adult human fibroblasts by defined factors. Cell. 2007;131(5):861-72.
13. Meissner A, Wernig M, Jaenisch R. Direct reprogramming of genetically unmodified fibroblasts into pluripotent stem cells. Nat Biotechnol. 2007;25(10):1177-81.
14. Okita K, Ichisaka T, Yamanaka S. Generation of germline-competent induced pluripotent stem cells. Nature. 2007; 448(7151):313-7.
15. Park IH, Zhao R, West JA, Yabuuchi A, Huo H, Ince TA, et al. Reprogramming of human somatic cells to pluripotency with defined factors. Nature. 2008;451(7175): 141-6.
16. Yu J, Vodyanik MA, Smuga-Otto K, Antosiewicz-Bourget J, Frane JL, Tian S, et al. Induced pluripotent stem cell lines derived from human somatic cells. Science. 2007;318(5858):1917-20.
17. Morishima T, Watanabe K, Niwa A, Fujino H, Matsubara H, Adachi S, et al. Neutrophil differentiation from human-induced pluripotent stem cells. J Cell Physiol. 2011;226(5):1283-91.
18. Niwa A, Heike T, Umeda K, Oshima K, Kato I, Sakai H, et al. A novel serum-free monolayer culture for orderly hematopoietic differentiation of human pluripotent cells via mesodermal progenitors. PLoS One. 2011;6(7):e22261.
19. Matsubara K, Imai K, Okada S, Miki M, Ishikawa N, Tsumura M, et al. Severe developmental delay and epilepsy in a Japanese patient with severe congenital neutropenia due to HAX1 deficiency. Haematologica. 2007;92(12):e123-5.
20. Skokowa J, Fobiwe JP, Dan L, Thakur BK, Welte K. Neutrophil elastase is severely down-regulated in severe congenital neutropenia independent of ELA2 or HAX1 mutations but dependent on LEF-1. Blood. 2009;114(14):3044-51.
21. Kobayashi M, Yumiba C, Kawaguchi Y, Tanaka Y, Ueda K, Komazawa Y, et al. Abnormal responses of myeloid progenitor cells to recombinant human colony-stimulating factors in congenital neutropenia. Blood. 1990;75(11):2143-9.
22. Konishi N, Kobayashi M, Miyagawa S, Sato T, Katoh O, Ueda K. Defective proliferation of primitive myeloid progenitor cells in patients with severe congenital neutropenia. Blood. 1999;94(12):4077-83.
23. Germeshausen M, Grudzien M, Zeidler C, Abdollahpour H, Yetgin S, Rezaei N, et al. Novel HAX1 mutations in patients with severe congenital neutropenia reveal isoform-dependent genotype-phenotype associations. Blood. 2008;111(10):4954-7.
24. Hiramoto T, Ebihara Y, Mizoguchi Y, Nakamura K, Yamaguchi K, Ueno K, et al. Wnt3a stimulates maturation of impaired neutrophils developed from severe congenital neutropenia patient-derived pluripotent stem cells. Proc Natl Acad Sci USA. 2013; 110(8):3023-8.
25. Hacein-Bey-Abina S, Von Kalle C, Schmidt M, McCormack MP, Wulffraat N, Leboulch P, et al. LMO2-associated clonal T cell proliferation in two patients after gene therapy for SCID-X1. Science. 2003;302(5644):415-9.
26. Ott MG, Schmidt M, Schwarzwaelder K, Stein S, Siler U, Koehl U, et al. Correction of X-linked chronic granulomatous disease by gene therapy, augmented by insertional activation of MDS1-EVI1, PRDM16 or SETBP1. Nat Med. 2006;12(4):401-9.
27. Howe SJ, Mansour MR, Schwarzwaelder K, Bartholomae C, Hubank M, Kempski H, et al. Insertional mutagenesis combined with acquired somatic mutations causes leukemogenesis following gene therapy of SCID-X1 patients. J Clin Invest. 2008; 118(9):3143-50.
28. Cavazzana-Calvo M, Payen E, Negre O, Wang G, Hehir K, Fusil F, et al. Transfusion independence and HMGA2 activation after gene therapy of human beta-thalassaemia. Nature. 2010;467(7313):318-22.
29. Papapetrou EP, Lee G, Malani N, Setty M, Riviere I, Tirunagari LM, et al. Genomic safe harbors permit high beta-globin transgene expression in thalassemia induced pluripotent stem cells. Nat Biotechnol. 2011;29 (1):73-8.
30. Zou J, Sweeney CL, Chou BK, Choi U, Pan J, Wang H, et al. Oxidase-deficient neutrophils from X-linked chronic granulomatous disease iPS cells: functional correction by zinc finger nuclease-mediated safe harbor targeting. Blood. 2011;117(21):5561-72.
31. DeKelver RC, Choi VM, Moehle EA, Paschon DE, Hockemeyer D, Meijsing SH, et al. Functional genomics, proteomics, and regulatory DNA analysis in isogenic settings using zinc finger nuclease-driven transgenesis into a safe harbor locus in the human genome. Genome Res. 2010;20(8): 1133-42.
32. Hockemeyer D, Soldner F, Beard C, Gao Q, Mitalipova M, DeKelver RC, et al. Efficient targeting of expressed and silent genes in human ESCs and iPSCs using zinc-finger nucleases. Nat Biotechnol. 2009;27(9):851-7.
33. Henckaerts E, Dutheil N, Zeltner N, Kattman S, Kohlbrenner E, Ward P, et al. Site-specific integration of adeno-associated virus involves partial duplication of the target locus. Proc Natl Acad Sci USA. 2009;106(18):7571-6.
34. Ishikawa N, Okada S, Miki M, Shirao K, Kihara H, Tsumura M, et al. Neurodevelopmental abnormalities associated with severe congenital neutropenia due to the R86X mutation in the HAX1 gene. J Med Genet. 2008;45(12):802-7.

ELSEVIER

Brain & Development 36 (2014) 528–531

BRAIN & DEVELOPMENT
Official Journal of the Japanese Society of Child Neurology

www.elsevier.com/locate/braindev

Case report

Compound heterozygosity in *GPR56* with bilateral frontoparietal polymicrogyria

Yuji Fujii [a,*], Nobutsune Ishikawa [a], Yoshiyuki Kobayashi [a], Masao Kobayashi [a], Mitsuhiro Kato [b]

[a] *Department of Pediatrics, Hiroshima University Hospital, Hiroshima, Japan*
[b] *Department of Pediatrics, Yamagata University, Faculty of Medicine, Yamagata, Japan*

Received 24 May 2013; received in revised form 28 July 2013; accepted 31 July 2013

Abstract

Polymicrogyria is caused by a diverse etiology, one of which is gene mutation. At present, only one gene (*GPR56*) is known to cause polymicrogyria, which leads to a distinctive phenotype termed bilateral frontoparietal polymicrogyria (BFPP). BFPP is an autosomal recessive inherited human brain malformation with abnormal cortical lamination. Here, we identified compound heterozygous *GPR56* mutations in a patient with BFPP. The proband was a Japanese female born from non-consanguineous parents. She presented with mental retardation, developmental motor delay, epilepsy exhibiting the feature of Lennox–Gastaut syndrome, exotropia, bilateral polymicrogyria with a relatively spared perisylvian region, bilateral patchy-white-matter MRI signal changes, and hypoplastic pontine basis. *GPR56* sequence analysis revealed a c.107G>A substitution leading to a p.S36N, and a c.113G>A leading to a p.R38Q. Although affected individuals with compound heterozygosity in *GPR56* have not been previously described, we presume that compound heterozygosity of these two mutations in a ligand binding domain within the extracellular N-terminus of protein could result in BFPP. In addition, we observed unusually less involvement of perisylvian cortex for polymicrogyria, and Lennox–Gastaut syndrome for epilepsy, which are likely common features in patients with BFPP caused by *GPR56* mutations.

Keywords: Polymicrogyria; Lennox–Gastaut; GPR56; Heterozygous mutation

1. Introduction

The autosomal recessive bilateral frontoparietal polymicrogyria (BFPP) is a well-characterized neuronal migration defect that shows bilateral polymicrogyria with an anterior to posterior gradient, bilateral patchy-white-matter MRI signal changes (without specific patterns), and brainstem or cerebellar hypoplasia. Patients with BFPP present with mental retardation, developmental motor delay, seizures, ataxia, and dysconjugate gaze [1]. The causative gene for BFPP is the G protein-coupled receptor 56 gene (*GPR56*) [2]. GPR56 is one of the adhesion G protein-coupled receptors (GPCRs). Like other members of the adhesion GPCRs, GPR56 has an unusually long N-terminal extracellular domain that contains a high percentage of serine and threonine residues and a GPCR proteolytic site domain just before the first transmembrane spanning domain [3,4]. The serine and threonine-rich region can serve as an O- and/or N-glycosylation site [3,4].

So far, multiple independent mutations have been identified in *GPR56*, all of which are homozygous germline mutations. To date, 25 mutations in *GPR56*, including nine N-terminal extracellular domain mutations, are

* Corresponding author. Address: Department of Pediatrics, Hiroshima University Hospital, Faculty of Medicine, Hiroshima University, 1-2-3 Kasumi-cho, Hiroshima 734-8551, Japan. Tel.: +81 82 257 5212; fax: +81 82 257 5214.
E-mail address: yujinn0728@ybb.ne.jp (Y. Fujii).

0387-7604/$ - see front matter
http://dx.doi.org/10.1016/j.braindev.2013.07.015